NUMERICAL SIMULATION OF THIN MEMBRANES WITH CURVED CREASES

Kuruppu Achchige Lasith Hansaka Kuruppu

238037M

Master of Science (Major Component Research)

Department of Civil Engineering

Faculty of Engineering

University of Moratuwa

Sri Lanka

March 2025

NUMERICAL SIMULATION OF THIN MEMBRANES WITH CURVED CREASES

Kuruppu Achchige Lasith Hansaka Kuruppu

238037M

Thesis submitted in partial fulfillment of the requirements for the degree
Master of Science (Major Component Research)

Department of Civil Engineering
Faculty of Engineering

University of Moratuwa
Sri Lanka

March 2025

DECLARATION

I declare that this is my own work and this thesis does not incorporate without acknowledgement any material previously submitted for a degree or diploma in any other University or Institute of higher learning and to the best of my knowledge and belief it does not contain any material previously published or written by another person except where the acknowledgement is made in the text. I retain the right to use this content in whole or part in future works (such as articles or books).

Signature: *UOM Verified Signature* Date: 2025-03-02

K.A.L.H. Kuruppu

The above candidate has carried out research for the Masters thesis under my supervision. I confirm that the declaration made above by the student is true and correct.

Name of Supervisor: Prof. H.M.Y.C. Mallikarachchi

Dr. H.M.S.T. Herath

Signature of the Supervisor: Date: 2025-03-03

…….. ……

Prof. H.M.Y.C. Mallikarachchi Dr. H.M.S.T. Herath

DEDICATION

I hereby dedicate this to my family and all the teachers who have been the backbone of my life.

ACKNOWLEDGMENT

I would like to extend my gratitude to all the personnel who have given their immense support throughout completing this thesis.

I would like to first and foremost thank my supervisors Prof Chinthaka Mallikarachchi and Dr Sumudu Herath for giving me unwavering support and dedication towards me and my work. Your support has been a great motivation for me, and I am thankful for the knowledge I gained under you.

Also, I hereby thank you for the help provided by the head of the department and all the lecturers of the Department of Civil Engineering for the guidance and help given to me.

Also, I would like to thank my family and friends for their immense support throughout this journey.

To all the others who helped me thank you again for your support. Without your help completion of this thesis would not have been possible.

Sincerely,

K.A.L.H. Kuruppu

ABSTRACT

Deployable membranes are commonly used in the construction of solar sails, solar arrays, and sun shields. These structures are fabricated on the ground and then deployed to their operational configuration in space. These structures are very large in dimensions but need to be compacted into a very small package that can be stowed inside a launch vehicle. Membrane structures are often folded using different crease patterns and wrapped around a central hub to achieve the compacted state. The thickness of the membranes place and important role in selecting a folding pattern as one length of the membrane increases with layers overlapping around the hub. To get a smooth wrap, a viable option is to change the crease pattern geometry to a curved crease with changing curvature to accommodate increased thickness. Changing the geometry into a curved crease pattern needs to be analyzed properly to understand its suitability for use in deployable membrane structures. This study analyzes the effectiveness of curved and straight crease wrapping structures. Two numerical models are used for the analysis of each crease pattern to understand behavior. The curved crease wrapping pattern shows good overall wrapping motion with less stresses in the initial stages when compared to the straight crease wrapping pattern. The stress is reduced up to 26% in the initial stages. Also, a crease idealization technique is introduced in this study to incorporate the self-opening behavior of the membrane creases into the numerical model. This idealization technique is further evaluated for a multiple crease geometry with a Miura-Ori model. The crease modeling technique shows a good overall fit with the experimental results validating the numerical simulations.

Keywords: Deployable structures, membrane, wrapping structures, curved crease

TABLE OF CONTENTS

Declaration i

Dedication ii

Acknowledgment iii

Abstract iv

Table of Contents v

List of Figures vii

List of Tables ix

Chapter 1 1

Introduction 1

1.1 Deployable Membrane Structures 1

1.2 Thickness Effect on Spirally Folded Membrane Structures 1

1.3 Scope and Aim 3

1.4 Chapter Organization 4

Chapter 2 5

Literature Review 5

2.1 Spirally Stowed Straight Crease Membranes 5

2.2. Studies on Spirally Stowed Curved Crease Membranes 7

2.3. Analysis of Crease Folding Structures 9

2.3.1. Straight Crease Folding Mechanics 9

2.3.2. Curved Crease Folding Mechanics 9

2.4. Numerical Simulation Techniques of Wrapping Structures 10

Chapter 3 11

Geometry of Curved Crease Wraps 11

3.1 Impact of Membrane Thickness on Folding 11

3.2 Generation of Curved Crease to Accommodate Thickness 12

3.3 Selected Geometry 13

Chapter 4 17

Experimental Analysis of Self-Opening Behavior for Multiple-Creased Structures 17

4.1. Crease Mechanics of a Folded Membrane 17

4.2 Miura-Ori Specimen Preparation 19
4.3 Miura-Ori Folding Experiments 20
4.4. Miura-Ori Experiment Results Analysis 21
Chapter 5 24
Simulation of Crease Folding Behavior 24
5.1. Connector Definitions and Stiffness Assignment 24
5.2. Miura-Ori FEM Model 25
5.2.1 Model Details 27
5.2.2 Abaqus/Standard Simulation Implementation 28
5.3 Analysis of Numerical Simulation Results 29
Chapter 6 31
Simulation of Curved Crease Wrapping Structure 31
6.1 Experimental Setup and Results 31
6.2 Numerical Modelling of a Single Curved Crease Fold 32
6.3 Numerical Modelling of Wrapping Structure 35
6.4 Numerical Model Results 36
Chapter 7 39
Conclusions and Future Work 39
References 41

LIST OF FIGURES

Figure 1.1 Geometric effects due to the thickness of panels 2
Figure 1.2 Bulging storage 2
Figure 1.3 Different folding and wrapping patterns 3
Figure 2.1 Guest and Pellegrino's spiral folding pattern 5
Figure 2.2 Scheel's fold pattern 6
Figure 2.3 Circumferential folding pattern 6
Figure 2.4 Circumferential folding pattern folding steps 7
Figure 2.5 Curved creases for spiral folding pattern 7
Figure 2.6 Beech leaf pattern 8
Figure 2.7 Spiral folding pattern 8
Figure 2.8 Two developable surfaces assembled through a developability constraint 9
Figure 3.1 Effective thickness approximations 11
Figure 3.2 Flat and folded geometry relationship 13
Figure 3.3 Variation of S and theta 14
Figure 3.4 Generated crease in radial coordinate system 15
Figure 3.5 Placement of creases parallelly 15
Figure 3.6 Constructed spiral folding pattern 16
Figure 4.1 Behavior of a crease 17
Figure 4.2 Moment rotation curves 18
Figure 4.3 Predicted rotational stiffness value respect to thickness 19
Figure 4.4 Specimen preparation 19
Figure 4.5 Miura-Ori specimen details 20
Figure 4.6 Experimental apparatus for Miura-Ori folding 21
Figure 4.7 300HN experimental results analysis 22
Figure 4.8 Experimental results of force vs displacement 200HN and 300HN 22
Figure 4.9 Experimental results of force vs displacement with vertex cut 200HN and 300HN 23
Figure 5.1 Single crease model 24
Figure 5.2 Numerical model geometry 26
Figure 5.3 Mesh sensitivity analysis for Miura-Ori model 26

Figure 5.4 Stages of folding simulations..... 27
Figure 5.5 Numerical model energy variations..... 28
Figure 5.6 Experimental and numerical results comparison..... 29
Figure 5.7 Experimental vs explicit numerical model results comparison 30
Figure 6.1 Spiral folding pattern membrane model deployed and wrapped state..... 31
Figure 6.2 Bottom view and side view during deployment 32
Figure 6.3 Single curved crease fold model boundary conditions..... 32
Figure 6.4 Number of discretization along the crease..... 33
Figure 6.5 Mesh sensitivity analysis for a curved crease..... 34
Figure 6.6 Different connector arrangements with gaps..... 34
Figure 6.7 Strain energy maximum value vs no of connector elements 35
Figure 6.8 Wrapping patterns..... 36
Figure 6.9 - Numerical model details..... 37
Figure 6.10 Experimental vs numerical results..... 37
Figure 6.11 Comparison of straight and curved crease numerical model results 38

LIST OF TABLES

Table 3.1 Wrapping pattern geometric properties..... 14
Table 5.1 Material properties 26
Table 6.1 Experimental model properties 31

CHAPTER 1

INTRODUCTION

Large space structures are becoming popular for various planetary missions as well as terrestrial applications ranging from military to civil across the globe. Deployable structures are preferred in space applications due to their ability to stow in a small volume and then deploy into a larger structure. Some examples of the deployable structures used are deployable antennas [1], [2], solar sails [3], [4], booms [5], [6], and solar arrays [7], [8]. Several deployable structures are being used which are made of different kinds of materials to achieve specific objectives.

1.1 Deployable Membrane Structures

A common deployable structure type which is used in space applications such as solar sails, solar arrays, and sun shields are membrane structures. These structures possess a higher packaging efficiency, lightweight, effective deployment ability, and compaction ability which are required for space applications.

These space structures require a larger surface area when they are deployed in space, but the structure is required to be transported from Earth to space using a launch vehicle [9]. For that, the structure needs to be effectively compacted into a smaller volume without damaging it. Different kinds of folding patterns are being used to effectively compact the membrane and then to deploy it without damaging the membrane. Many of these folding patterns are influenced by the art Origami paper folding [10], [11] which is used to shape the developable surfaces into different kinds of folds.

This Origami concept is then coupled with engineering understanding along with bioinspired concepts [12], [13] to further develop more effective patterns for deployable structures. One is spiral folding patterns which are inspired by flower blooming. In these structures, the membrane is folded or wrapped around a hub placed in the middle of the membrane. Different types of crease patterns are used to fold the membrane and effectively wrap it around the hub. The membranes have thickness and the impact from the thickness to the folded shape needs to be investigated.

1.2 Thickness Effect on Spirally Folded Membrane Structures

Thickness of the panels is not considered in the initially presented designs like the folding pattern proposed by Guest which only shows a geometric construction of the pattern. Therefore, the zero thickness panel assumption gives perfect folding, which is unrealistic in the actual behavior as in Fig. 1.1 [14].

Thickness accommodation is mainly required during the stowage stage where the increasing thickness due to wrapping or folding of the membrane needs to be considered. With each iteration, the wrapped or folded membrane is placed on top of the previous layer and the thickness of the previous layer affects the stowing radius. Therefore, ignoring change in diameter affects the membrane stowing process, leading to poor repeatable storage configurations, and an increase in the final stored volume and stress concentrations in the membrane. Therefore, the thickness of the membrane

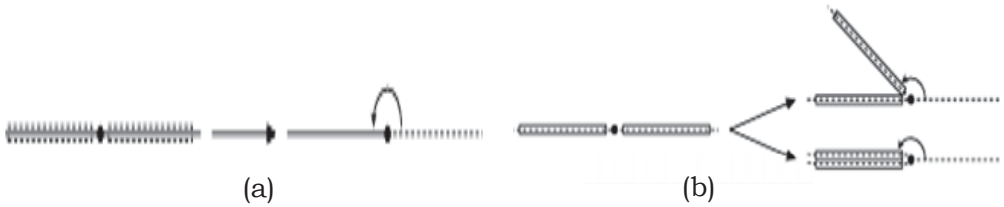

Fig. 1.1: Geometric effects due to the thickness of panels [14] (a) idealized structure (b) actual structure

needs to be considered during the wrapping of spiral folding structures.

There are several methods that are being used in accommodating the thickness of the membrane wraps. Compression-compliant structures [15] approximation is one method that uses bridge sections to connect the membrane parts. A similar method is used in shear shear-compliant method where the parallel Z-fold strips are connected through bridge sections which allows the parallel membrane parts to adjust and slip to get a compacted wrap during the folding. Similar methods are presented by Greschik [16] which uses a completely stripped connection between the membrane layers and by Manan Arya [17] which uses a slipping fold between the connection of membrane strips to achieve a slipping motion during the wrapping process. Also, as in Fig. 1.2 Sakamoto et al [16] proposed the bulging storage method where the membrane is bulged when wrapping around the central hub which leads to an increase in storage volume.

The next approach is to change the creases' shape in the membrane structure to accommodate the increasing wrapped radius of the structure. Here the crease shape is changed along its longitudinal direction by changing its curvature but for considering

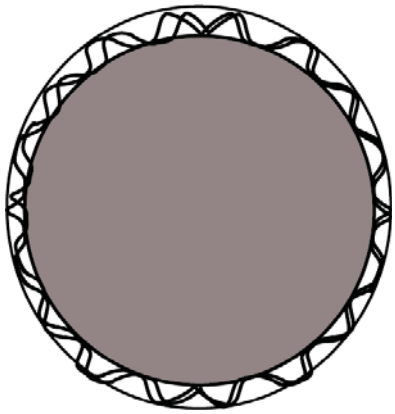

Fig. 1.2: Bulging storage

the construction easiness these curvature changes are assumed as piecewise linear lines. Guest proposed a modification to change the crease lines into piecewise linear lines which gives a curved shape which is shown in Fig. 1.3 (a), and similar methods were also proposed by Liyanage[14]. In this piecewise approximation, there are still drawbacks to the membrane as stress concentrations can occur at the line vertices, leading to damage to the membrane structure.

So, a more viable option is to move into fully curved creases. Natori and Yamamoto [18] have developed curved crease-wrapping structures to overcome those thickness effects. The thickness effect during the wrapping is considered when the membrane is stowed around the structure. The creases of the spirally folding pattern are changed along with the crease length by changing the curvature to accommodate that extra thickness increment which is shown in Fig. 1.3 (b). The focus on using curved creases instead of straight crease lines is not properly analyzed in the case of spirally folded deployable structures.

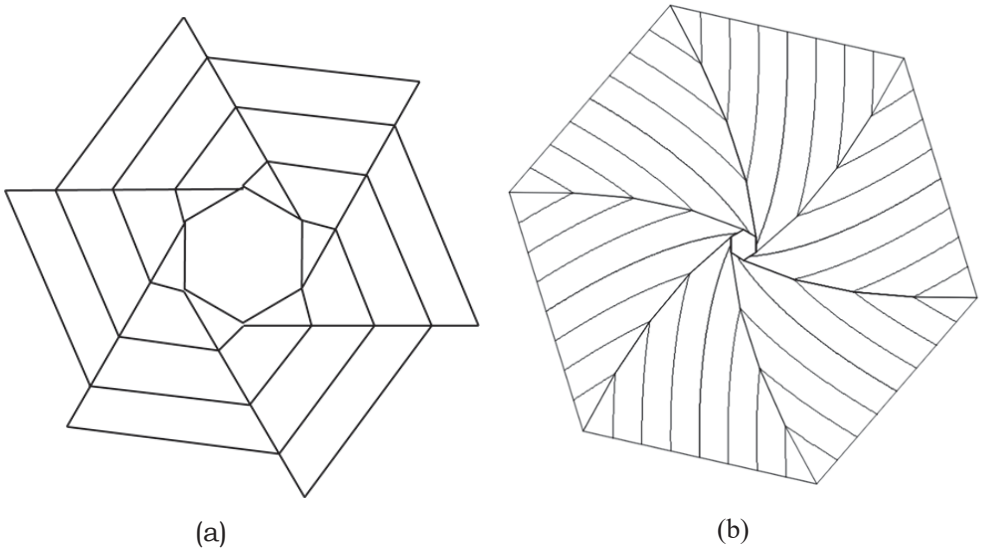

Fig. 1.3: Different folding and wrapping patterns (a) spiral fold pattern by Guest and Pellegrino (b) spiral folding pattern by Natori

1.3 Scope and Aim

The broad aim of this research is to study the impact of changing creases from straight to curved in deployable wrapping structures. This understanding is required to evaluate the suitability of using curved creases. In past literature, the curved crease wraps provide a good compaction relative to straight crease patterns. Analyzing only the compaction is insufficient in assessing the suitability of crease shape. The stress variations and the deformations during folding are not properly analyzed. So, the impact of changing crease geometry needs to be studied in the sense of stress distributions in the structure, stowed volume, and geometrical deformations.

The impact of the crease geometry change is analyzed as a numerical simulation by studying curved and straight crease wrapping patterns. The same dimension membrane structure is designed as a curved crease pattern and a straight crease pattern and wrapped around a central hub. Initially, a new crease idealization technique is presented in the study to incorporate self-opening behavior into creases, and its applicability in multiple creased structures is tested. The self-opening behavior is simulated in a finite element model for the Miura-Ori structure and evaluated with experimental results. Then curved and straight crease-wrapping structures during the initial wrapping stages are analyzed using numerical modelling.

Straight crease and curved crease wrapping structures are modeled as finite element models using the Abaqus/Standard package to evaluate their performance under the above-mentioned factors.

1.4 Chapter Organization

This thesis consists of seven chapters. Following the initial introduction chapter, Chapter 2 provides a comprehensive literature review on the deployable spirally wrapped structure, crease pattern geometry construction, and numerical analysis methods. Specific focus is given to the construction of the geometry of rotationally skew fold pattern geometry.

Chapter 3 explains the thickness effect in the membrane wrapping structures and the implemented crease geometry modification technique. The geometry construction for selected dimensions is then explained in the latter part of the chapter.

Chapter 4 provides an experimental analysis of the self-opening behavior of a multiple-creased structure. A Miura-Ori specimen is analyzed experimentally for this study by observing the force vs displacement behavior and results from the experiment are further discussed in the latter part of the chapter.

Chapter 5 provides a comprehensive analysis of the crease idealization techniques and the implementation of self-opening behavior to the numerical model. Then the results are assessed for the experimental Miura-Ori folding experiments.

Chapter 6 describes modeling of the wrapping structures. Experimental results taken from the literature are used to assess the simulation technique. The straight and curved crease wrapping model results are discussed in the latter part.

Chapter 7 concludes the thesis and present future research suggestions.

CHAPTER 2

LITERATURE REVIEW

2.1 Spirally Stowed Straight Crease Membranes

The deployable structures use folding patterns to achieve an effective compact state and the efficient deployment during the unfolding state. The spirally stowed structures also which can be called wrapping and folding structures are the most common deployable membrane structure type that is used in space structures. “Fold” is named the pattern with quasi-rigid tessellations whereas “wrap” denotes patterns that smoothly bend. The most common crease geometry being used is straight creases.

This can be further classified by the straight crease folding pattern used in the membrane. There are three main crease pattern types identified which are used in membrane structures that are compacted around a central hub. The first pattern which was developed by Guest and Pellegrino [19] is used to fold the membrane around a polygonal hub and can be called a spiral fold pattern which is shown in Fig. 2.1. The panels quasi rigid panels where the primary motion is the crease folding. In a rigid panel structure, the panel's primary deformation is only the folding at the crease but in a membrane structure panel bending also happens. Hence quasi-rigid folding panels are possible for this folding pattern and also suitable for membranes.

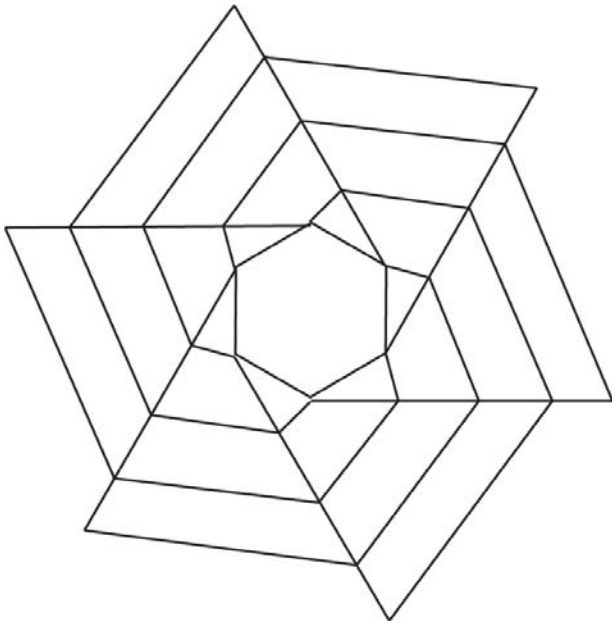

Fig. 2.1: Guest and Pellegrino's spiral folding pattern

Scheel [20] presented a wrapping pattern in Fig. 2.2 where the membrane wraps around the central hub. Variation of this pattern is then presented by Hiroshi Furuya [15] called “rotationally skew fold” where the panels bend after the initial folding. This pattern is further researched by Natori [21] who constructed a wrapping pattern that

has a changing curvature to accommodate thickness change resulting a curved-shaped creases. This wrapping pattern consists of two stowage mechanisms, where the membrane is folded along the crease lines and then the folded panels are simultaneously wrapped around the central hub. The stored height of the membrane structure is equal to the distance between the parallel fold lines. Hence, the stored height is independent of the membrane diameter which provides a good compacted stowed configuration.

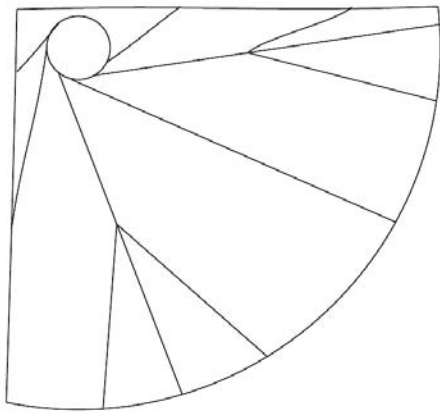

Fig. 2.2: Scheel's fold pattern

Other than the above two methods circumferential folding pattern which is shown in Fig. 2.3 is presented by Natori et al [22] which was used in origamisat1.

The actual stowage mechanism is a wrapping motion around the central hub as shown in Fig. 2.4.

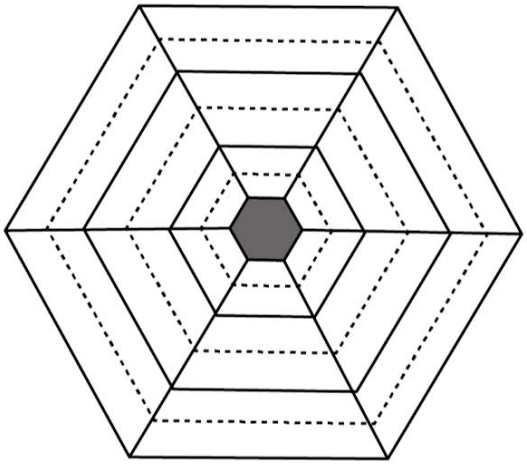

Fig. 2.3: Circumferential folding pattern

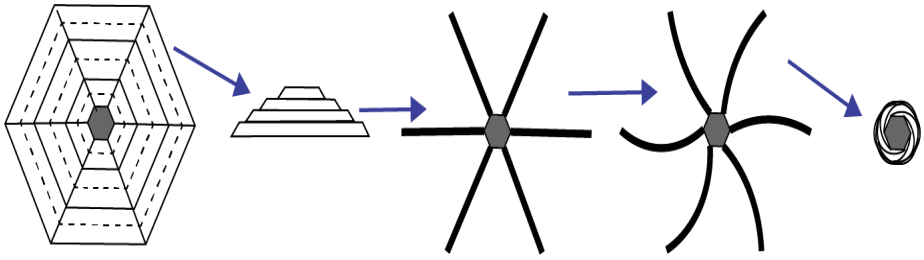

Fig. 2.4: Circumferential folding pattern folding steps

2.2. Studies on Spirally Stowed Curved Crease Membranes

The spirally stowed straight crease patterns described in the previous part can be modified to accommodate the thickness effect during the stowage stage. This can be done by changing the crease curvature of the membrane structure to match the radius increment due to the wrapped membrane around the central hub.

The curvilinear pattern proposed by Guest and Pellegrino [19] and the circumferential folding pattern can be modified to a curved crease structure as in Fig. 2.5. The straight creases in the initial designs are changed into curved creases to accommodate the thickness.

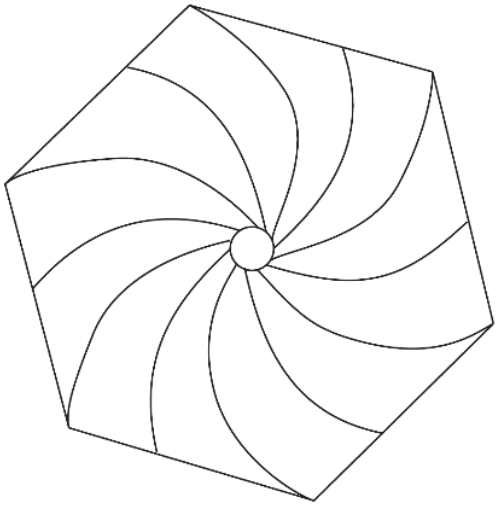

Fig. 2.5: Curved creases for spiral folding pattern

The wrapping patterns can also be modified to accommodate the thickness effect. Lee and Pellegrino presented a curved crease geometry taking inspiration from the straight crease pattern developed by analyzing the beech leaf fold [23], [24]. The membrane is first folded in as a Z-fold and then wrapped around the central hub and the curvature of the crease is changed to accommodate the changing thickness as shown in Fig. 2.6.

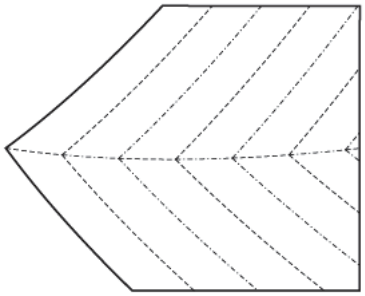

(a)

(b)

Fig. 2.6: Beech leaf pattern (a) pattern geometry (b) wrapping steps in beach leaf pattern [24]

This inspired Nicolas Lee and Sigrid Close to develop a curved crease pattern that can be used to effectively wrap a square sheet around a hub [25].

Natori further modified the wrapping pattern initially proposed by Furuya to accommodate the thickness effect by constructing equations to accommodate the thickness effect. This pattern is named the "spiral folding pattern" by Natori [21] which is presented in Fig. 2.7. The readers should note this pattern is identified in this paper as a wrapping pattern although it is named as a "spiral folding pattern". This is because the stowage of the membrane around the hub is a wrapping motion which is different from the Guest and Pellegrino's "spiral fold" pattern where the primary stowing motion is a folding around the hub.

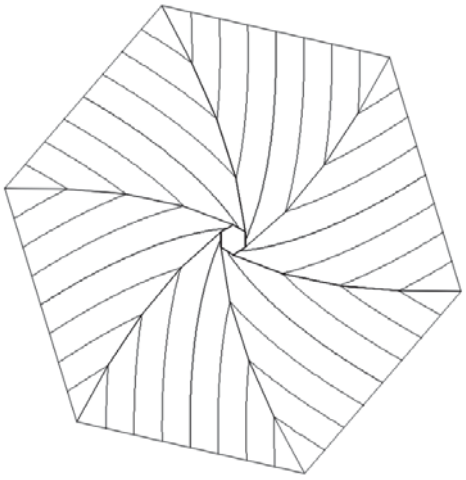

Fig. 2.7: Spiral folding pattern

2.3. Analysis of Crease Folding Structures

2.3.1. Straight Crease Folding Mechanics

The straight crease folds are influenced by an ancient paper folding technique called Origami. To form a straight crease origami pattern, it is required to maintain developability quality. A surface with zero Gaussian curvature forms a developable surface.

The Gaussian curvature (K) is the product of the principal curvatures κ_1 and κ_2, and it presents smooth surface characteristics.

$$K = \kappa_1 \kappa_2$$

The plane curvature (κ) at a point is,

$$\kappa = \frac{1}{\rho} = \frac{d\theta}{ds}$$

where ρ represents a circle which shares the same curvature and tangent which is known as the radii of curvature. This can be represented as the change of the tangent angle $d\theta$ concerning the line segment ds.

Origami surfaces are generated by combining two or more developable surfaces connected through the crease line. As an example, repetitive parallelogram planes which are developable surfaces make the Miura pattern.

2.3.2. Curved Crease Folding Mechanics

Curved crease folds are derived from the straight crease origami folds where the crease is converted into a curved shape. Knowledge of developability and origami surfaces provides a building block to effectively understand curved crease folds. In Fig. 2.8 a

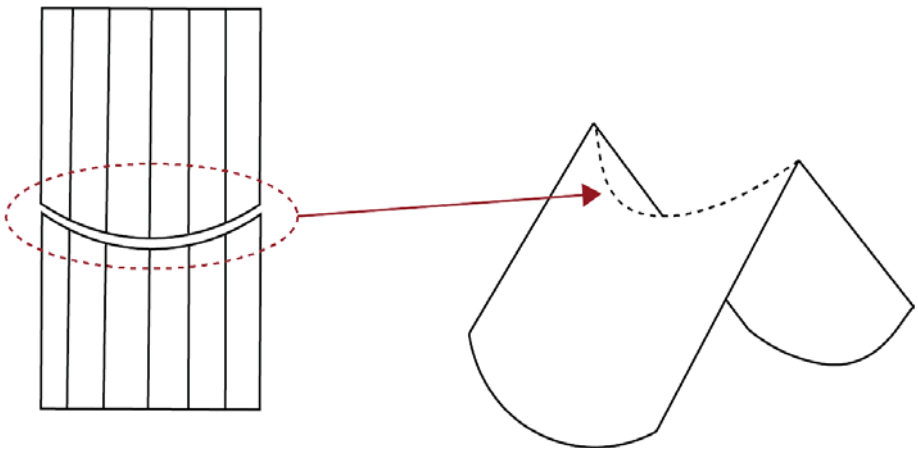

Fig. 2.8: Two developable surfaces assembled through a common developability constraint

curved crease is used to connect two curved developable surfaces forming a curved crease origami structure which can be called a curved crease fold.

Curved crease folding is a combination of crease folding and panel bending. Hence the energy stored during the curved crease folding is stored as potential energy due to those two motions. The assembly of different developable surfaces makes different folded 3D configurations. These configurations are the minimum bending energy configurations [5].

The bending energy stored due to bending if a developable surface is,

$$U_b = \frac{1}{2}\int_A D_b k_1^2 \, dA,$$

where D_b gives the bending stiffness, k_1 is the non-zero principal curvature and A is the area of the developable surface. D_b is given by,

$$D_b = \frac{Et^3}{12(1-v^2)}$$

where E is the modulus of elasticity, v is the poisons ratio and t is the thickness of the membrane [26].

2.4. Numerical Simulation Techniques of Wrapping Structures

Deployable wrapping structure simulation needs to be done to simulate both the wrapping and unwrapping simulations accurately. The geometrical modeling of the wrapping structure is insufficient to show these structures' actual behavior in action. The insertion of structural properties and proper idealizations in the simulation shows accurate behavior, otherwise, it may lead to deployment problems in space like in the IKAROS deployment [20].

Parque and Miyashita [27] modeled the wrapping simulation of the spiral folding structure with a Graphical Processing Unit [28]. In this method a bar and hinge explicit simulation technique is used to simulate the wrapping.

Okuizumi and Yamamoto simulated the wrapping of the same spiral folding structure using a spring-mass system model [18]. This model effectively simulates the folded state where the crease behavior is further added to the numerical model to accurately simulate the wrapping behavior along with the buckling strength of the structure, damping, and air drag. Lin et al [29] simulated wrapping simulation for straight crease structures using finite element simulation.

CHAPTER 3

GEOMETRY OF CURVED CREASE WRAPS

The method proposed by Natori [21] to design a curved crease wrapping pattern to accommodate the thickness change while wrapping is presented in this chapter. In the latter part, a geometric design is made from an experimental demonstration to construct a wrapping pattern that is used in the numerical model generation to simulate the wrapping behavior.

3.1 Impact of Membrane Thickness on Folding

The important consideration of this geometry construction is the thickness of the membrane. Here in this method, the membrane thickness (T) is not merely the actual membrane thickness but an effective thickness (t). This is introduced due to the bending of the membrane around the folding point. The actual thickness is larger than the membrane thickness as in Fig. 3.1.

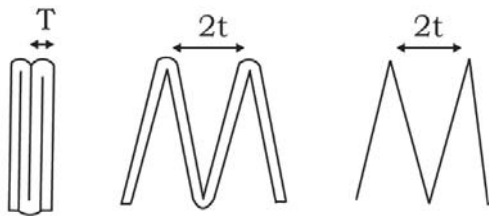

Fig. 3.1: Effective thickness approximations

From here onwards the effective thickness of the membrane is considered as ***t*** and used for all the geometry construction equations. Parque and Miyashita [27] presented the same pattern construction method by Natori in a more clarified way. The geometry construction method below is presented to construct the pattern.

In the geometry construction process, the following parameters first need to be introduced.

N – Central polygonal hub number of sides

R_0 – Apothem of the Central hub polygon

R_f – Apothem of the membrane outer polygon

H – Height of the folded configuration

Considering the infinitesimal part in Fig. 3.2 the relationship between polar tangential angle ϕ, infinitesimal angle $d\theta$, and infinitesimal distance dR is as follows,

$$\tan(\phi) = \frac{Rd\theta}{dR}$$

Here θ is the polar angle and $R \in [R_0, R_f]$.

The ϕ value varies along the R and it is required to find relationships between them. b is the breath and S denotes the length of a zigzag on the same plane in the folding process.

$$\frac{dS}{S} = -\tan(\phi)\, d\theta$$

Then k value is defined for the central hub which has N number of edges.

$$k = N \tan\left(\frac{\pi}{N}\right)$$

The area of a polygon is krR^2 and the circumference is $2kR$. Note that the k in a polygon is similar to π of a circle. The following equation is obtained from the transformation of the infinitesimal element and the similarity ratio of the perimeter change in Fig. 3.2.

$$\frac{2\pi r}{2kR} = \sqrt{\sin^2\phi + \left(\frac{t}{S}\right)^2}$$

3.2 Generation of Curved Crease to Accommodate Thickness

Using a similar relation between the upper face area of the wrapped membrane cylinder $2\pi r dr$ and the polygonal area $2kRdR$ we get this equation,

$$\frac{2\pi r dr}{2kRdR} = \frac{t}{S\cos\phi}$$

Using the above equations the following equation is obtained for ϕ,

$$\phi = \sin\left(\frac{\sqrt{(\pi rS + kRt)(\pi rS - kRt)}}{SkR}\right)$$

Then the following three differential equations are constructed using the above relationships to find the values of $\theta, S \; and \; r$ values with respect to R.

$$\frac{d\theta}{dR} = \frac{1}{R}\left(\frac{\sqrt{(\pi rS + kRt)(\pi rS - kRt)}}{SkR\sqrt{\left(\frac{t}{S}\right)^2 - \left(\frac{\pi r}{kR}\right)^2 + 1}}\right)$$

$$\frac{dS}{dR} = \frac{-a}{Sk^2R^3}\left(\frac{(\pi rS + kRt)(\pi rS - kRt)}{\left(\frac{t}{S}\right)^2 - \left(\frac{\pi r}{kR}\right)^2 + 1}\right)$$

$$\frac{dr}{dR} = \frac{Rkt}{\pi Sr\sqrt{\left(\frac{t}{S}\right)^2 - \left(\frac{\pi r}{kR}\right)^2 + 1}}$$

To solve the equations the initial conditions are as follows,

$$\theta_0 = \frac{2i\pi}{N},$$

where, $i \in [0, N-1]$

$$S_0 = H,$$

$$R_0 = r_0.$$

The coordinates of the folding line A which starts from the midpoint of each side of the central polygonal hub are given in (R, θ). Lines A1 are parallel to line A.

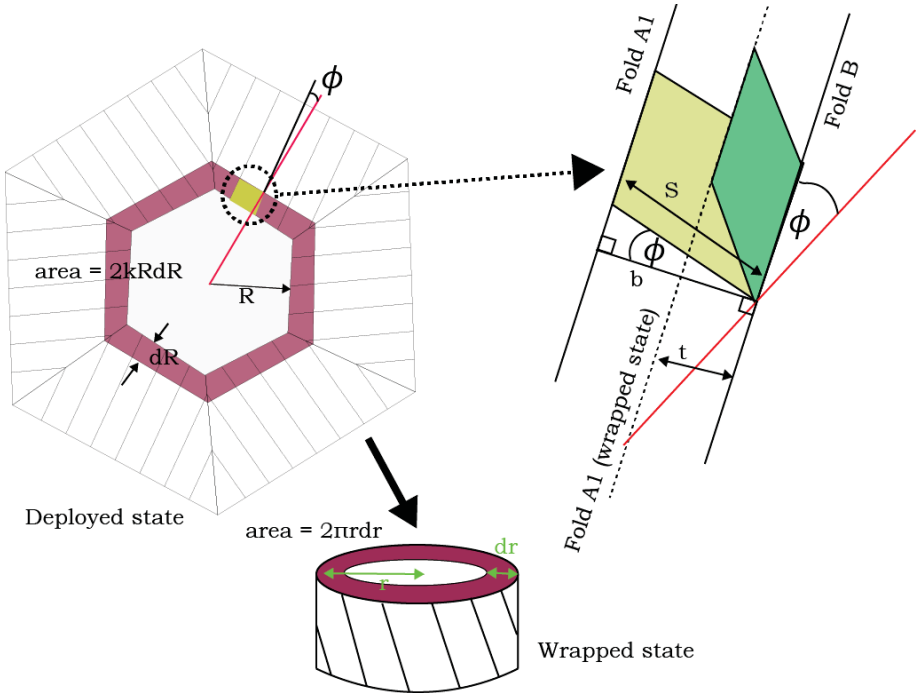

Fig. 3.2: Flat and folded geometry relationship

3.3 Selected Geometry

The wrapping structure for the analysis needs to be simulated with the Abaqus finite element package. The first step is to construct geometry for the wrapping pattern.

Values for geometry are taken from Yamamoto's experimental setup [18] which is presented in Table 3.1. The membrane thickness of the experimental is 7.5 μm but the effective thickness of the membrane panels is taken as 1 mm.

Table 3.1: Wrapping pattern geometric properties

Length of diagonal folding line	650 mm
Thickness of membrane	7.5 μm
Inner radius of the stowed shape	20 mm
Stowed height	45 mm
Gap between folded membrane layers	1 mm

The other variable values that are selected for the construction of geometry are listed as below, N = 6, t = 1 mm, H = 45 mm, S_0 = H , R_0 = 20 mm, r_0 = R_0 and R_c = 375.27 mm. After solving the differential equations the geometrical properties are shown in Fig. 3.3.

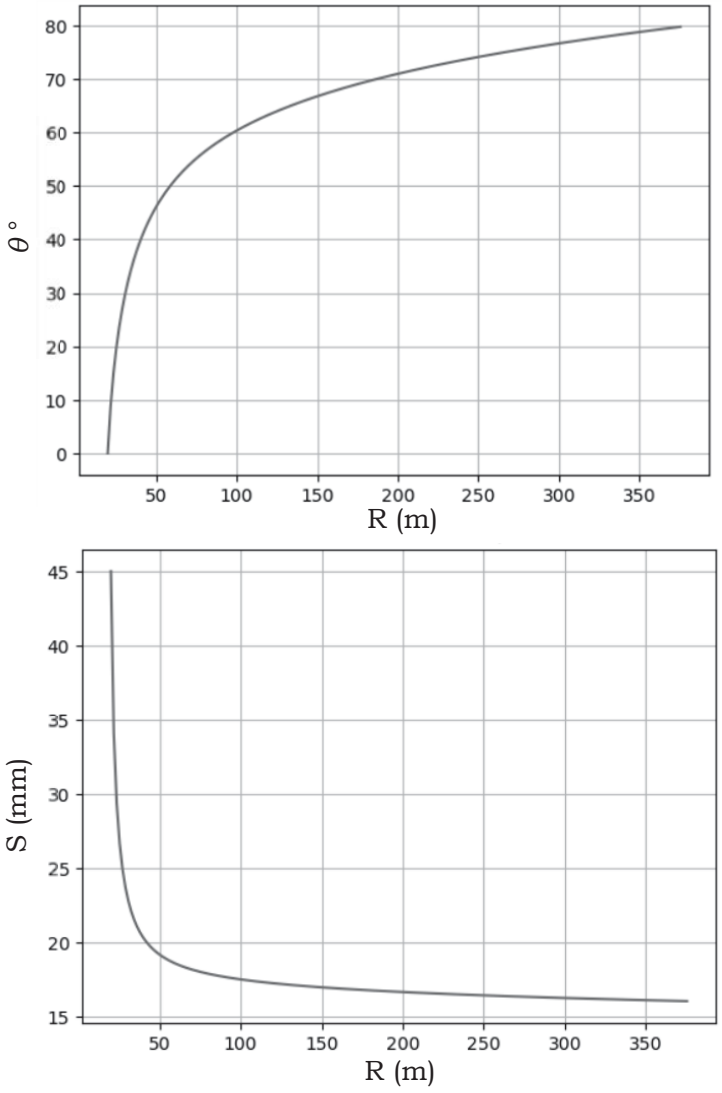

Fig. 3.3: Variation of S and theta (θ)

The generated crease in the radial coordinates system is presented in Fig. 3.4. After the crease creation as in Fig. 3.5, the next step is to tesselate creases to make the full curved crease folding pattern. For that, a part of the wrapping structure is selected. Then creases are placed parallel to the initial crease line which is marked in red color with an offset of 45 mm. The line starts from the midpoint of the central hexagonal hub.

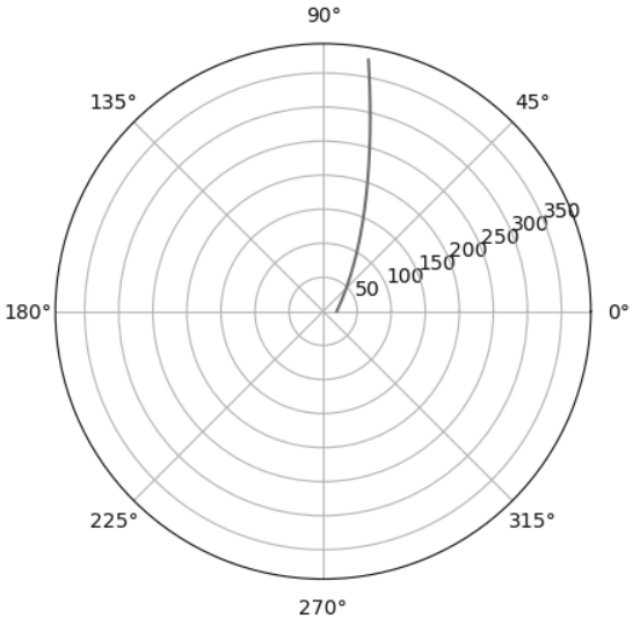

Fig. 3.4: Generated crease in radial coordinate system

Then the triangular side is placed around the central hub for six directions to form the wrapping membrane structure which is shown in Fig. 3.6.

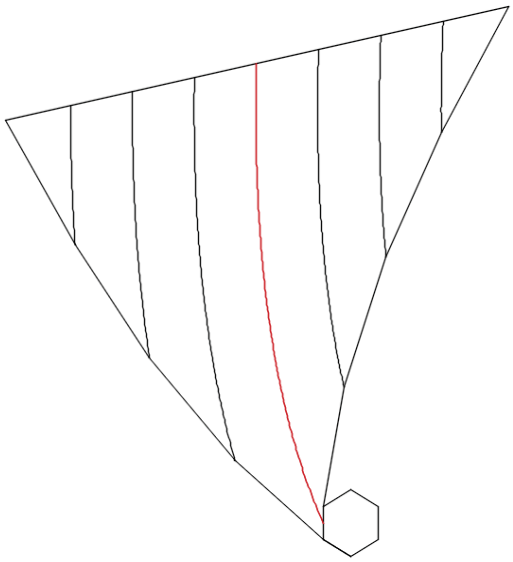

Fig. 3.5: Placement of creases parallelly

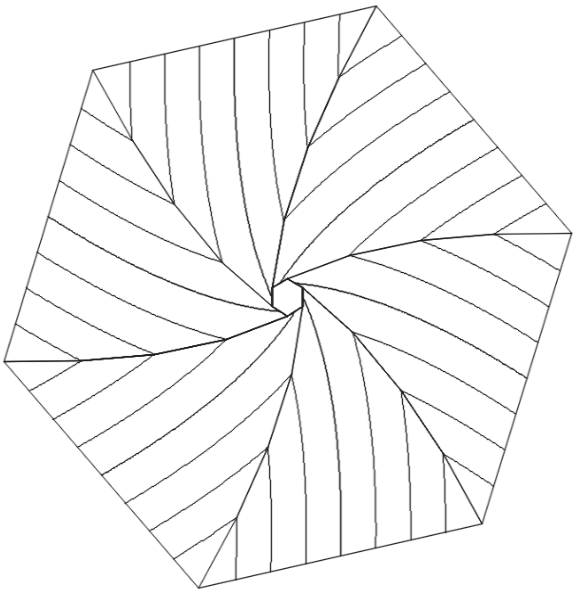

Fig. 3.6: Constructed spiral folding pattern

CHAPTER 4

EXPERIMENTAL ANALYSIS OF SELF-OPENING BEHAVIOR FOR MULTIPLE-CREASED STRUCTURES

Membrane folding structures can be considered as a combination of a crease and membrane panels. This combination gives a unique behavior to membrane folds which is different from folding structures with rigid panels and ideal hinges. The behavior of a single crease is first presented in this chapter and the application to a combination of creases is analyzed with a Miura-Ori experimental study in the latter part of the chapter.

4.1. Crease Mechanics of a Folded Membrane

In deployable membrane structures to precisely compact the membranes are folded along the fold lines. When the fold is in an elastically deformed state it is called a bend and when plastic deformations occur it is called a crease [30]

The thin membrane is creased and released from loading it opens into a stress-free state as in Fig. 4.1. This phenomenon is called self-opening and the angle it opens is called neutral angle.

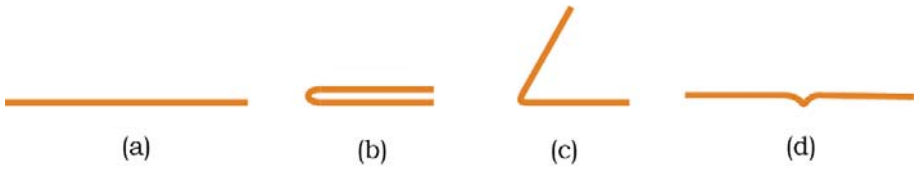

Fig. 4.1: Behavior of a crease (a) uncreased membrane (b) fully folded state during creasing (c) neutal state (d) forced opened state

This crease behavior is idealized to a rotational spring which is connected by two panels. The rotational spring behavior can be characterized by the following equation where θ, M, ϕ_0 and k denotes the rotational angle, the moment in the spring, the neutral angle, and rotational stiffness respectively [30]

$$M = k(\theta - \phi_0)$$

The self-opening behavior is captured by Sutharsanan[31] in previous experiments using a Kapton membrane with three thicknesses. A Kapton membrane with 20 mm × 40 mm is folded along the midline and placed 7.05 kg load for 30 minutes to form a crease. After creasing the specimens were left for 24 hours to self-open into the neutral angle state. The moment required to fold the specimen and the angle at each folding increment was recorded to capture the moment rotation relationship of the crease which is presented in Fig. 4.2.

The location where the moment becomes zero is where the membrane is opened into a neutral state. The angle at this location is considered the neutral angle. Then the self-opening angle is recorded, and the crease stiffness values of the crease are taken from the gradient of the plot. These figures capture the self-opening region of the fold. The same crease stiffness is also assumed for the forced opening region where the angle between panels is larger than the neutral angle for the study in this paper. The recorded self-opening angles are 104° for 200 HN and 99° for 300 HN.

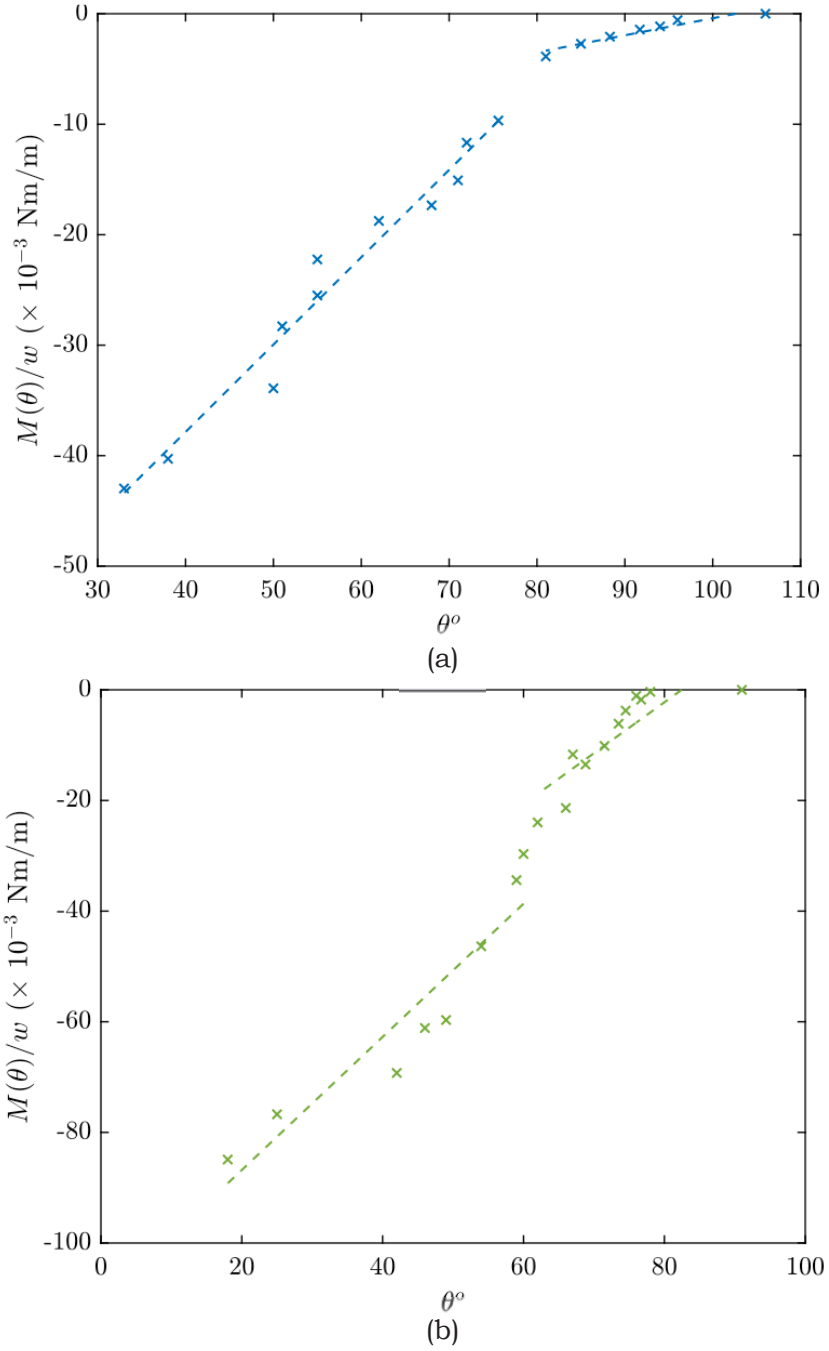

Fig. 4.2: Moment rotation curves for (a) 200 HN (b) 300 HN [31]

The values taken for the crease stiffness are plotted in Fig. 4.3 to the thickness of the membrane. The trendline is then plotted with cubic fit to the thickness and this helps to assume the value for crease stiffness of a Kapton membrane which is formed using the same procedure.

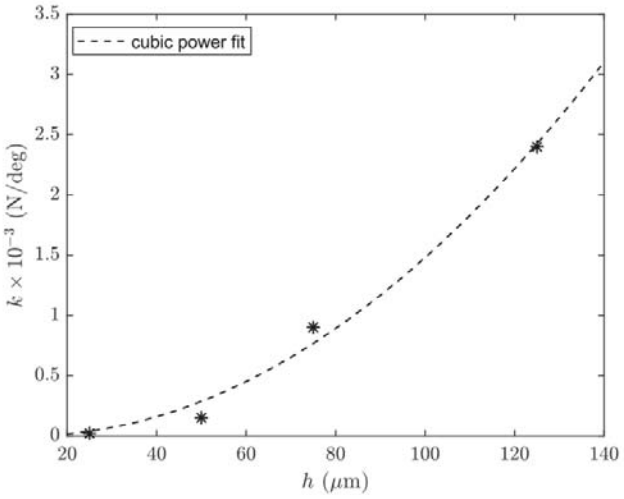

Fig. 4.3: Predicted rotational stiffness value respect to thickness

4.2 Miura-Ori Specimen Preparation

The experimental study conducted in this regard aims to verify the accuracy of the idealization technique used in the numerical study. Folding and unfolding behavior of multiple creased Miura-Ori unit cells with two different thicknesses, 50.08 µm (200HN) and 76.2 µm (300HN), were conducted and steps are shown in Fig. 4.4.

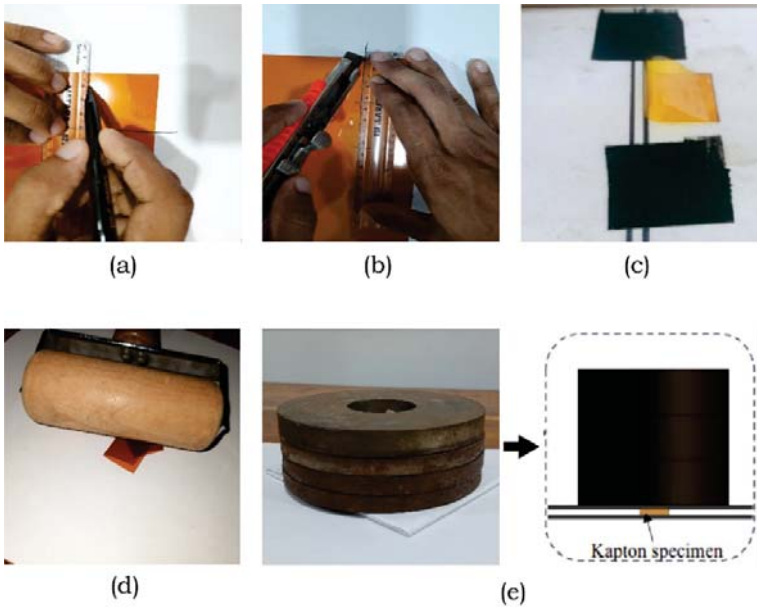

Fig. 4.4: Specimen preparation (a) marking dimensions (b) cutting specimens (c) folding specimens (d) preloading using roller (e) loading using 7.05 kg

The dimensions of the Miura Ori structure were marked on the polyimide film and cut into smooth edges using a sharp knife. The specimen was first pre-creased using a 174g wooden roller by placing it on top of specimens for 3 minutes. Then a 7.05 kg load was placed on top of the pre-creased specimen for 30 minutes to form the creases. Here the force applied to the creasing is changed to get a more localized load transfer to the crease. If the loading is applied via a larger metal plate it does not effectively transfer the loading only to the crease. This affects the crease stiffness value compared to a single crease, folded using the same load. To apply the 7.05 kg load to crease the specimens, a 30 mm × 30 mm metal plate was used which transferred a higher portion of load to the creases. Then, the specimens were allowed to relax for 24 hours after creasing. Fig. 4.5 shows the not-creased Miura-Ori unit cell and its stable state after creasing.

4.3 Miura-Ori Folding Experiments

The experimental apparatus, as shown in Fig. 4.6, comprises a 3D printed "Optimus Mega" linear actuator attached to an MG996R servo motor to provide smooth linear motion for folding and unfolding the specimen. The actuator, controllable via the Arduino platform, serves to convert rotary motion into linear motion. The specimen was mounted on an electronic balance capable of measuring reaction forces with a minimum reading of 0.0001 g. During folding, the scale reading increases, and during unfolding, the scale reading decreases, as it was preloaded with a known weight.

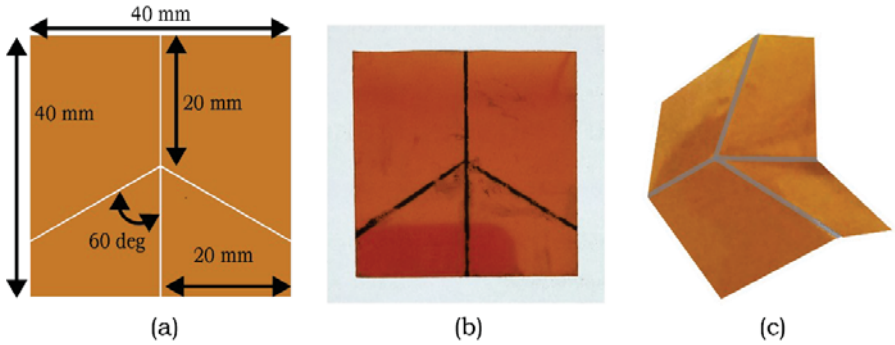

Fig. 4.5: Miura-Ori specimen details (a) specimen dimensions (b) uncreased specimen (c) stable Miura-Ori specimen after creasing

A dial gauge capable of measuring displacements with a minimum reading of 0.01 mm was used to measure the linear displacements. The specimen was placed between two 5 mm wide v notches made of Aluminium strips on either side which were attached to the support on the electronic balance at one side and the linear actuator at the other side. Using the linear actuator, displacement control was applied to one edge of the specimen. The dial gauge was placed on the linear actuator arm to measure the displacements. 5 mm wide thin Sellotape strips were used to hold the specimen at both notches to prevent slipping during the experiments. The bending effect of the thin Sellotape was assumed negligible during the experiments, allowing the boundary conditions to be approximated as pinned in the numerical model.

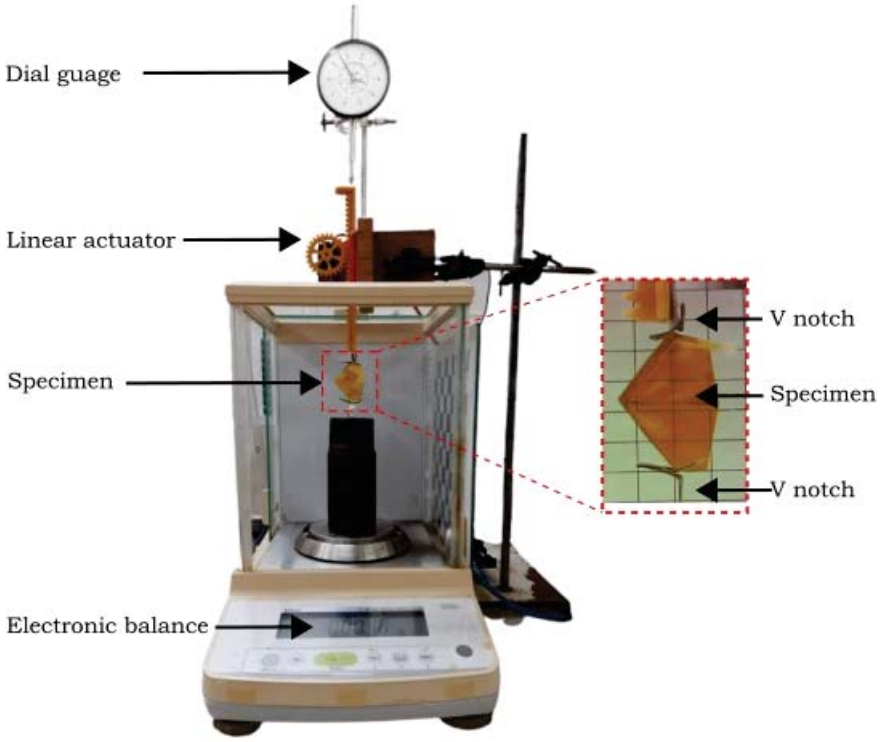

Fig. 4.6: Experimental apparatus for Miura – Ori folding

First, the specimen and support were placed on top of the electronic scale without connecting to the linear actuator, and the scale reading was set to zero. This way, the weight of the specimen and the support were excluded from the scale readings. Then, the specimen was connected to the linear actuator, with the initial starting position as the self-opened neutral state. Then linear actuator was used to apply linear displacements to the specific men. Starting from the neutral state, the folding motion was captured for 12 mm downwards. Then 12 mm unfolding motion was captured for upward direction starting from the fully folded state. Readings from the scale and dial gauge were recorded for each step. Experiments were repeated three times for two similar specimens to ensure better accuracy and the most accurate results were taken into the analysis.

4.4. Miura-Ori Experiment Results Analysis

The analysis of the Miura-Ori experimental folding is compared with the folding curve of the 300HN specimen in Fig. 4.7. The experiment started from the neutral state ‘A’ to the folded state ‘E’ as shown. In the ‘A’ location, the structure is in the neutral state without any stresses with the force recorded close to zero. With the applied displacement the force got increased. In locations ‘A’ to ‘B’ the two panels of the Miura-Ori structure appear to be straight. The crease folding was prominent in the folding motion instead of the bending of the panels. In this region, the gradient of the graph is almost linear. After point ‘C’ and moving to point ‘D’ the panels started to bend along with the crease folding. This was observed with the change of gradient

after point ‘C’ in the graph. Up to point ‘E’ the force increased with significant panel bending as in the figure. Moving to points ‘D’ to `E' the force increased due to both panel bending and crease folding behavior.

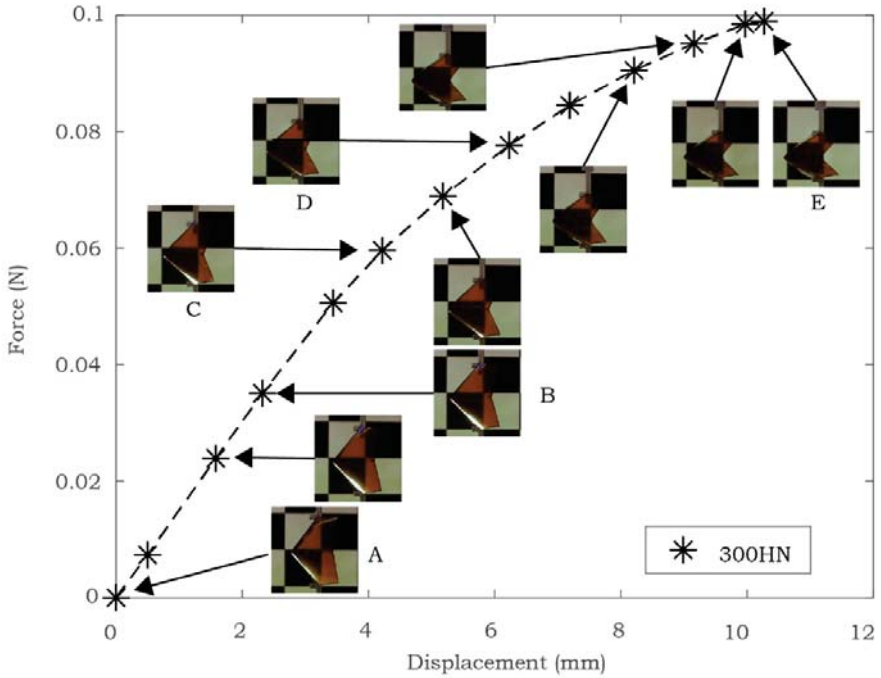

Fig. 4.7: 300HN experimental results analysis

Fig. 4.8 shows the displacement vs force plot of the Miura-Ori specimen during folding and unfolding. The first iteration represents a pre-loading state, and it is not taken for the analysis. The region above the Force = 0 represents the folding stage and

The crease intersection at the middle of the structure was also constructed with a cut

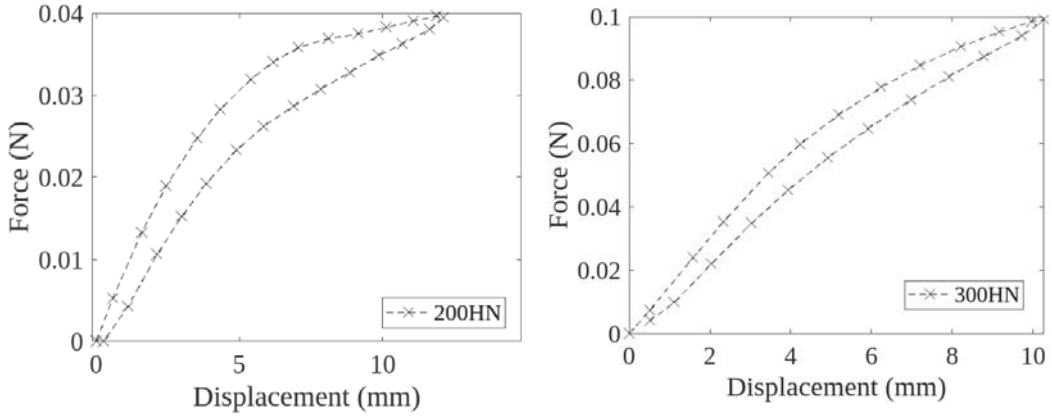

Fig. 4.8: Experimental results of force vs displacement 200HN and 300HN

at the mid-vertice point. This is done to provide a similar behavior to the numerical idealizations of the Miura-Ori structure which is comprehensively explained in the

next chapter. Notably, the force required for folding and deployment behavior is further reduced due to these modifications as in Fig. 4.9.

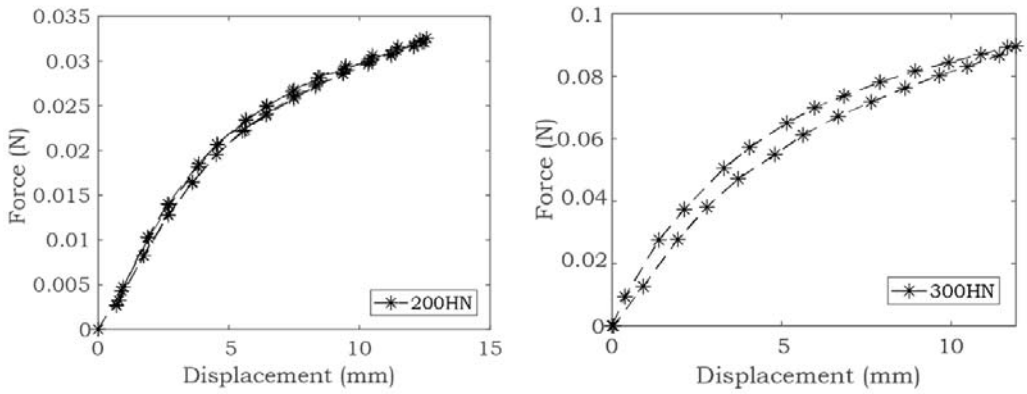

Fig. 4.9: Experimental results of force vs displacement with vertex cut 200HN and 300HN

CHAPTER 5

SIMULATION OF CREASE FOLDING BEHAVIOR

The unique behavior of creases characterized in the previous study needs to be accurately incorporated into numerical studies to simulate the actual behavior of folds. In this chapter, the method and idealizations followed to incorporate this behavior are discussed along with a result comparison.

5.1. Connector Definitions and Stiffness Assignment

The Revolute connector is used to simulate the idealization of the rotational spring behavior of the crease. The neutral angle opening behavior is incorporated into the revolute connector by defining the moment vs rotation graph values.

The moment-angle relationship was specified as linear. The Revolute connector allows rotational freedom in one direction while constraining the rotation in the other two directions. The revolute connector configuration is shown in Fig. 5.1.

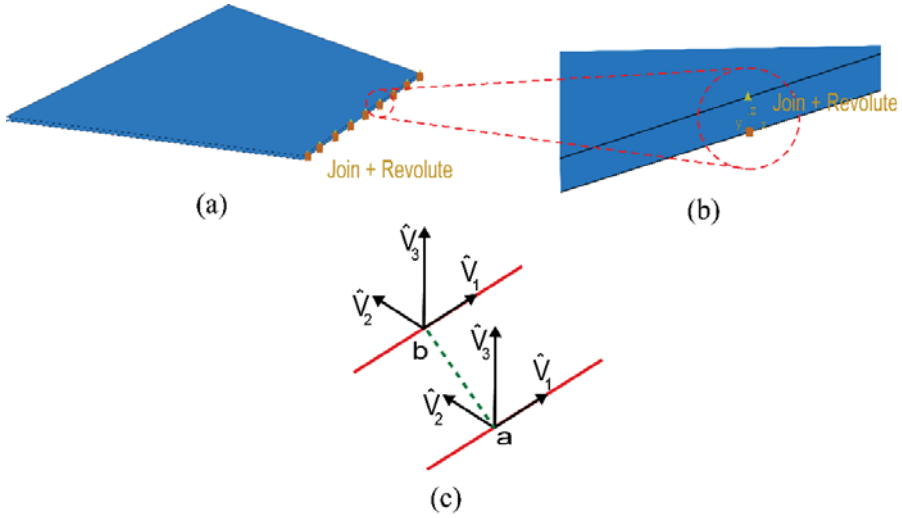

Fig. 5.1: Single crease model (a) fully folded initial state (b) connector elelment (c) connector elelemnt notations

For 200HN and 300HN are thick Kapton membranes the crease stiffness values are taken as 0.00012 N/degrees and 0.0009 N/degrees, respectively, from the experimental study conducted by Suthrasanan [31].

Both nodes ‘a’ and ‘b’ of a Revolute connector as in Fig. 5.1 can rotate around the shared 1-axis. The constrained rotational directions are,

$$\widehat{V_1^a} \cdot \widehat{V_2^b} = 0 \text{ and } \widehat{V_1^a} \cdot \widehat{V_3^b} = 0$$

The rotational angle θ of the node ‘b’ relative to node ‘a’ is measured as,

$$\theta = -\tan^{-1}\left(\frac{\widehat{V_2^a}\cdot\widehat{V_3^b}}{\widehat{V_3^a}\cdot\widehat{V_3^b}}\right)$$

Here θ is measured in the anticlockwise direction from $\widehat{V_2^a}$ to $\widehat{V_2^b}$ around $\widehat{V_1^a}$. The kinematic moment of the Revolute connector at node `a' is given by,

$$M = M_1\widehat{V_1^a}$$

Then ϕ_0 value is taken as 99 degrees from the experimental results. The moment is calculated by multiplying 0.00225 Nmm/degrees with the angle $(\theta - \phi_0)$ in degrees.

Then the values are inserted into the Abaqus Revolute connector definition where Moment and Rotation values for the connector are inserted in Nmm and Radians.

Then this equation is modified to match the Abaqus Revolute connection sign convention definition as follows,

$$\theta_1 = -\theta$$

$$M = M_1$$

$$M_1 = k(\theta_1 + \phi_0)$$

where the θ_1 and M_1 represent the angle and moment in the Abaqus nonlinear connector definition. The moment and rotations were inserted into the Abaqus Revolute connection stiffness definition as follows for the 300HN specimen with an ϕ_0 = 1.72788 rad (99 degrees).

5.2. Miura-Ori FEM Model

The idealization used for the crease behavior of the membrane needs to be validated for a multiple-creased structure to ensure its validity in practical applications. For that, a Miura-Ori structure is simulated in Abaqus/Standard FEM package. The single degree of freedom Miura-Ori structure is selected for its simplicity in the folding and unfolding behavior.

This simulation is carried out in 4 steps where in the initial step Miura-Ori model is simulated to self-open. This started from a fully folded state of the structure. Then a balancing step is modeled where the structure is pinned along its edges to dissipate its kinetic energy and become static. Then in the next step, it is folded and finally, it is forced to unfold.

The unfolded Miura-Ori unit cell is 40 mm × 40 mm in dimensions and consists of four panels as in Fig. 5.2. The distance between the panels is equal to the thickness of the membrane. All the dimensions are mentioned in Fig. 5.2.

The Miura-Ori structure was first modeled with S4R elements and S3R elements. The S4 elements produce more artificial energy, hence S3R elements were used to model the structure.

After careful study on mesh sensitivity comparing the last strain energy recorded at the end of the simulation as in Fig. 5.3 an element with a 1mm dimension was used

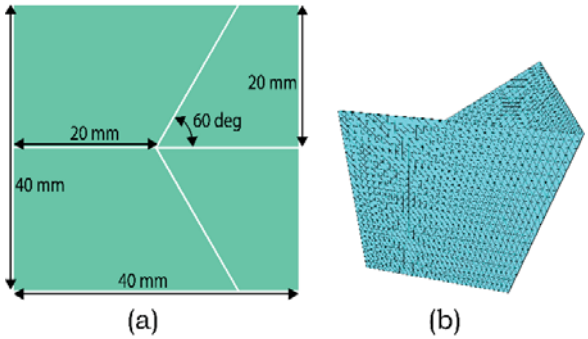

Fig. 5.2: Numerical model geometry (a) Miura-Ori model dimensions
(b) meshed Miura-Ori model

for the analysis. It gives 2900 nodes and 5376 S3R elements. The specimen is kept in between two rigid element panels. The material properties used for numerical study are mentioned in Table 5.1.

Table 5.1: Material properties

Density (kgm^{-3})	1420
Elastic modulus (MPa)	2760
Poisson's Ratio	0.34

As mentioned in the above section the crease idealization as a rotational spring is modeled in Abaqus finite element software using Join + Revolute connectors. The Join connection provides the panel relative movement restriction, and the Revolute connector provides the rotational stiffness. The dimensions of the creases of the Miura-

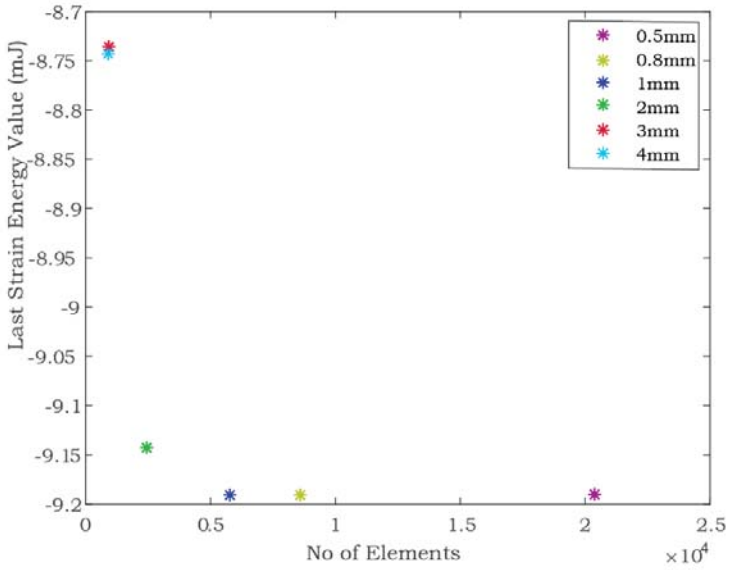

Fig. 5.3: Mesh sensitivity analysis for Miura-Ori model

Ori panel used here are identical in length. Hence the number of connectors along the creases was selected as 64 after a trial and error approach considering the stress variation along the crease.

5.2.1 Model Details

The different parts of the model come into contact with each other, and the *General contact* with *Normal Behaviour* and *Hard* Contact is assigned. The simulation of this Miura-Ori fold was conducted in four stages. In the initial step, the specimen is initiated from the fully folded state between two rigid plates as shown in Fig. 5.4 (a). Subsequently, one rigid plate is subjected to displacement while the other remains stationary, facilitating the self-opening of the specimen, as shown in Fig. 5.4 (b). The corresponding boundary conditions for each step are indicated in Fig. 5.4. In the third step, the folding process is simulated by applying downward displacement, as shown in Fig. 5.4 (c). The final step involved the unfolding process by applying displacement in the opposite direction. In steps 3 and 4, the boundary condition region and load application regions were replicated similar to the experimental study. The folding and unfolding processes are also conducted using two V-notches, mimicking the experimental setup as in Fig. 5.4 (d). Also, simulations are conducted with one model incorporating rotational stiffness connectors and another model using perfect hinges without any rotational stiffness, aiming to validate the significance of incorporating rotational stiffness.

The space between the rigid panels and the folded origami structure was equal to the thickness of a single Kapton specimen layer.

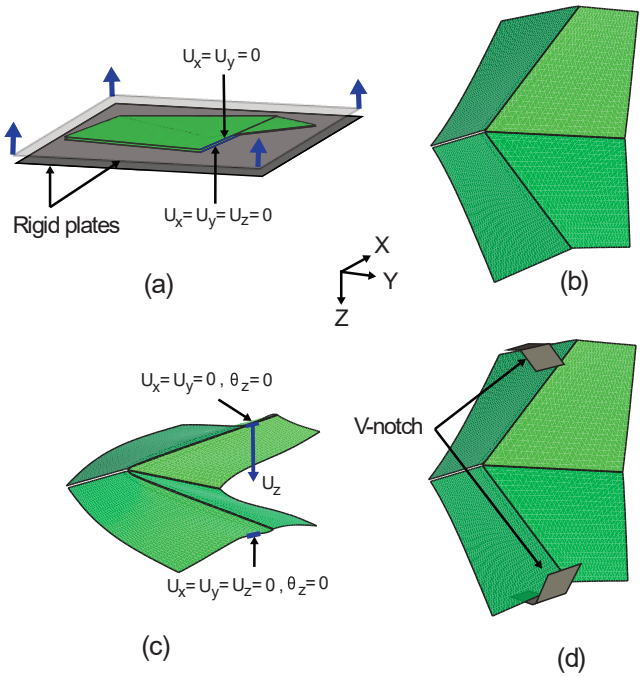

Fig. 5.4: Stages of folding simulations: (a) during self-opening step, (b) neutral state, (c) during folding step, (d) folding using notches

The edge of the Miura-Ori structure in the stationary plate has a pinned boundary connection. The moving edge has roller connections where displacement in X and Y directions is only restrained. The part of the edge closer to the creases is not assigned with boundary conditions to prevent any disturbance to the crease opening behavior. In the balancing step, the roller edge is also pinned at the deployed location and the structure is let to dissipate the kinetic energy to become static before starting the folding simulations. The simulation focused on the quasi-static state, requiring minimization of inertia forces. This is accomplished through the Abaqus/Standard Simulation Quasi-static application.

5.2.2 Abaqus/Standard Simulation Implementation

The simulation of a folding simulation of the Miura Ori structure observed an overlap in the first portion of the folding motion. With the increasing displacement, the difference between the force recorded in numerical and experimental simulations increased.

To increase accuracy all the simulations are conducted as quasi-static simulations in Abaqus dynamic implicit solver. This increases the efficiency of the analysis by reducing the time taken for the simulation. The notch angles of the simulation are also adjusted to increase the accuracy of the simulations to match the experimental apparatus. The energy distribution is presented in Fig. 5.5 where the artificial and kinetic energies are negligible compared to the internal energy of the model validation the motion is in quasi-static state during the folding and unfolding stages. The hike in the initial stage during the self-opening stage is neglected for the study as it is not compared with the experimental study.

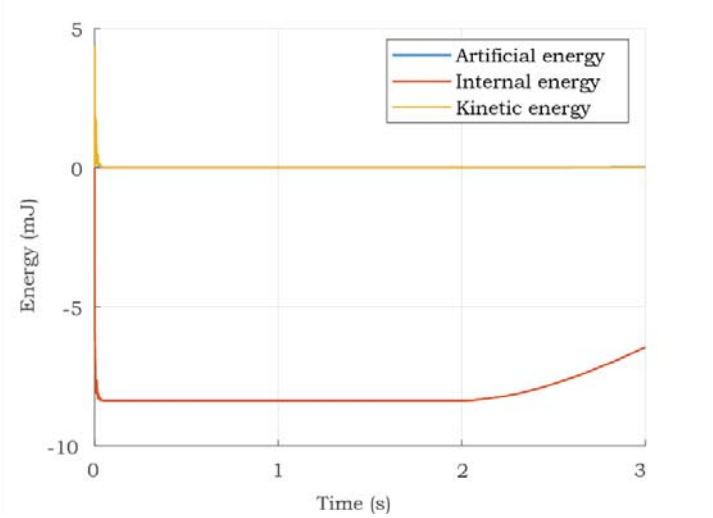

Fig. 5.5: Numerical model energy variations - 300HN

5.3 Analysis of Numerical Simulation Results

The unfolding curve of the numerical results is selected for comparison with the experimental results. The force vs displacement curve from the fully folded state to the forced opened state is compared in both thicknesses. The numerical model with no rotational stiffness at the crease notably has a minimal force recorded when compared with the experiments. The numerical model with crease stiffness shows a near alignment with the experiments showcasing the significance of idealizing the creases with rotational stiffness to get realistic simulation results.

In both experiments for 200HN and 300HN specimens, the force increment rate decreased in the initial part of the curve. As described in the previous section of this paper this occurred due to the panel bending along with the crease folding which is present in both the numerical models with rotational stiffness.

This can be seen in Fig. 5.6 where 300HN specimen experiment snapshots are compared with the numerical model with notches at the same displacement locations.

Again, after that, the force started increasing in experiments due to the metal notch supports causing bending in the Miura-Ori panels. This phenomenon is not present in models with pinned boundary conditions. When the two metal notches are modeled similarly to the experiment to fold the Miura-Ori structure, it shows a similar behavior as in experiments where the force increases. This is because panel bending occurs due to the notches' touching.

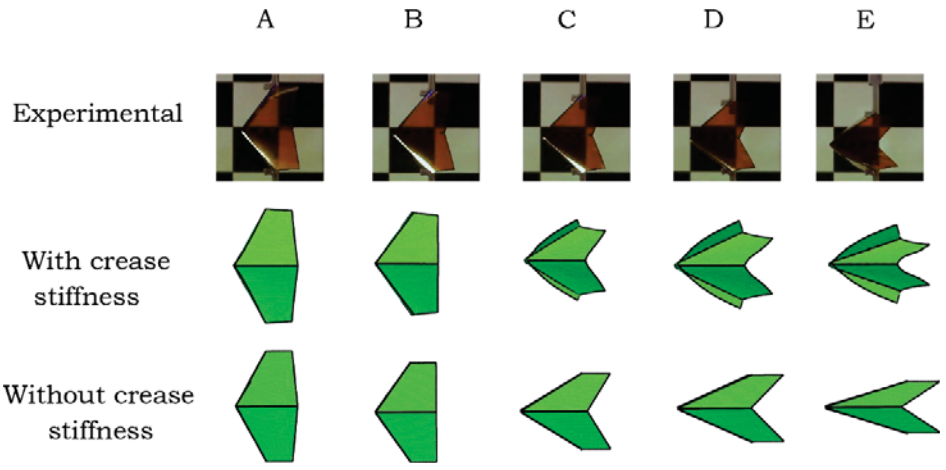

Fig. 5.6: Experimental and numerical results comparison

The unfolding curve of the numerical results is selected for comparison with the experimental results. The force vs displacement curve from the fully folded state to the forced opened state is compared in both thicknesses as in Fig. 5.7. The numerical model with no rotational stiffness at the crease notably has a minimal force recorded when compared with the experiments. The numerical model with crease stiffness shows a near alignment with the experiments showcasing the significance of idealizing the creases with rotational stiffness to get realistic simulation results.

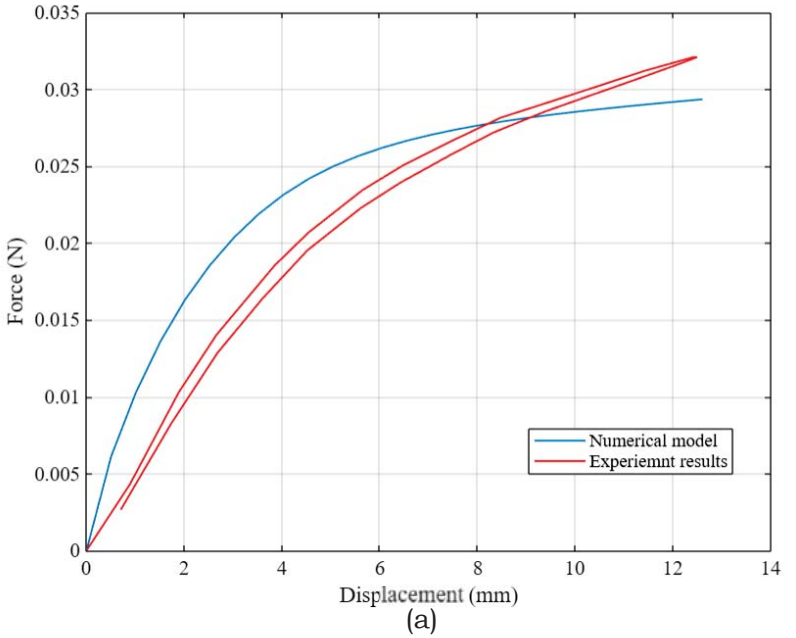

(a)

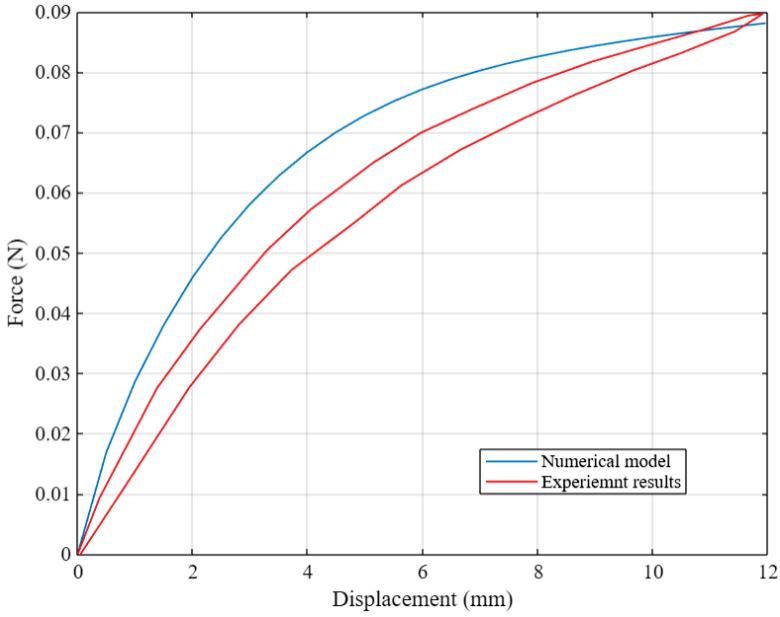

(b)

Fig. 5.7: Experimental vs explicit numerical model results comparison for (a) 200HN and (b) 300HN

CHAPTER 6

SIMULATION OF CURVED CREASE WRAPPING STRUCTURE

6.1 Experimental Setup and Results

A deployment experiment for a 7.5 μm polyimide film is conducted by Okuizumi et al [18]. The spiral folding pattern is used as the geometry for the experiment shown in Fig. 6.1. The flat surface is folded around the circular central hub forming a cylindrical folded shape. The design parameters of the wrapping pattern are shown in Table 6.1. The experiment is done in a vacuum chamber to reduce the impact of air resistance. The rotation speed of the central hub is placed at 3 Hz to reduce deformations from gravity. The deployment is captured from two cameras and quantified using image processing.

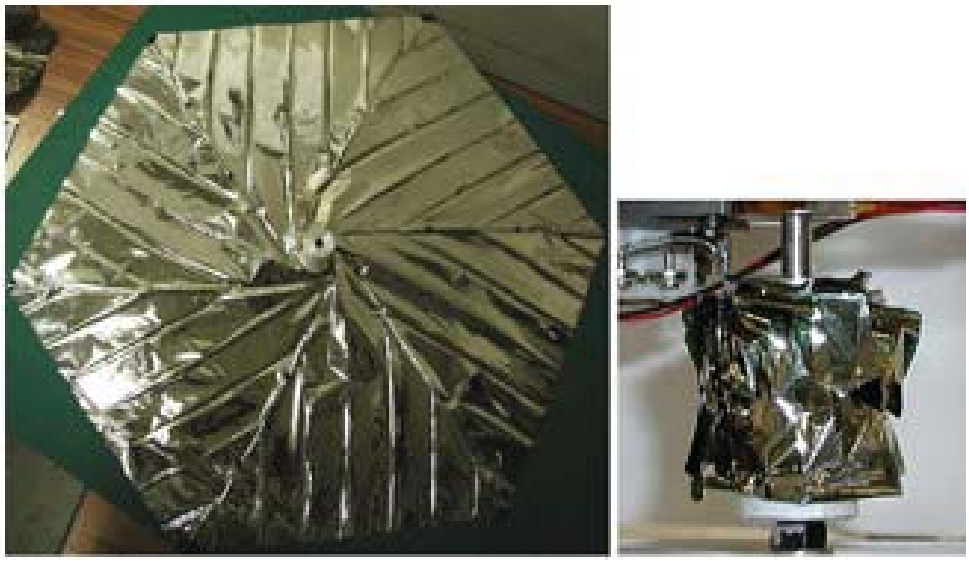

Fig. 6.1: Spiral folding pattern membrane model deployed and wrapped state [18]

Table 6.1: Experimental model properties

Elastic modulus	3.2 GPa
Poisson's ratio	0.34
Density	1420 kgm^{-3}

The deployment stages are shown in Fig. 6.2. The rate is equal to the ratio of the maximum radius of the membrane at a selected time to the original hexagon radius of

0.325 m. The maximum deployment is achieved after 0.9 seconds and up to that a liner deployment can be seen. After 0.9 sec, the membranes are unrolled excessively after maximum deployment.

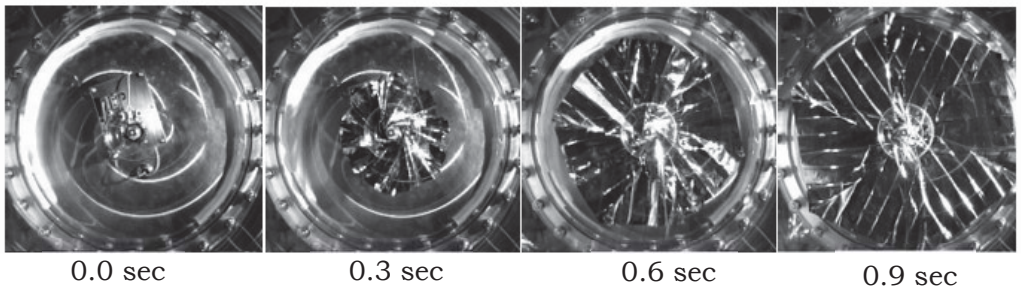

Fig. 6.2: Bottom view during deployment [18]

6.2 Numerical Modelling of a Single Curved Crease Fold

The crease generated from the differential equation is not a perfect curve line but a curvilinear line that contains several points. The number of points along the curve also contributes to the number of elements formed during the mesh creation. Therefore, a mesh sensitivity analysis was carried out by changing the number of discretization for a single curved crease fold like in Fig. 6.3 along the curved line. The initial crease line selected in the above section is placed parallel to each other in 45mm to form a curved strip as the geometry.

A displacement of 35 mm is applied along the central ridge crease. Out of four vertices at the bottom one is applied a pin joint while others are only restricted in Z direction movement.

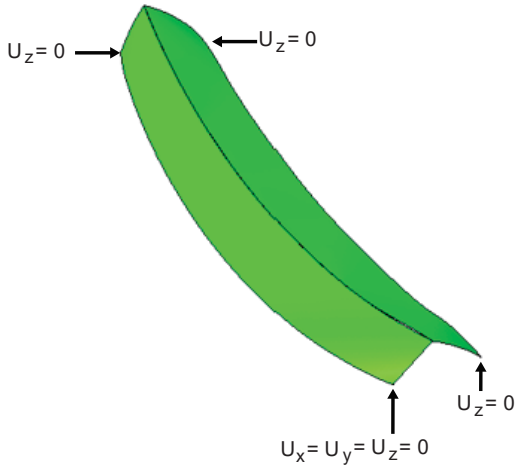

Fig. 6.3: Single curved crease fold model boundary conditions

The different stress variations of the structure along with changing discretization are presented in Fig. 6.4 and 6.5. After a careful mesh sensitivity study the 200 discretization along the crease were selected for the analysis which gives less than a 0.5% strain energy difference with the 500 discretization.

The crease stiffness value for the 7.5 µm polyimide film is assumed from Fig. 4.3. The cubic fit equation was used to calculate the crease stiffness value by substituting the membrane thickness to the equation. The crease stiffness value got was 4.92778×10^{-7} N/degrees.

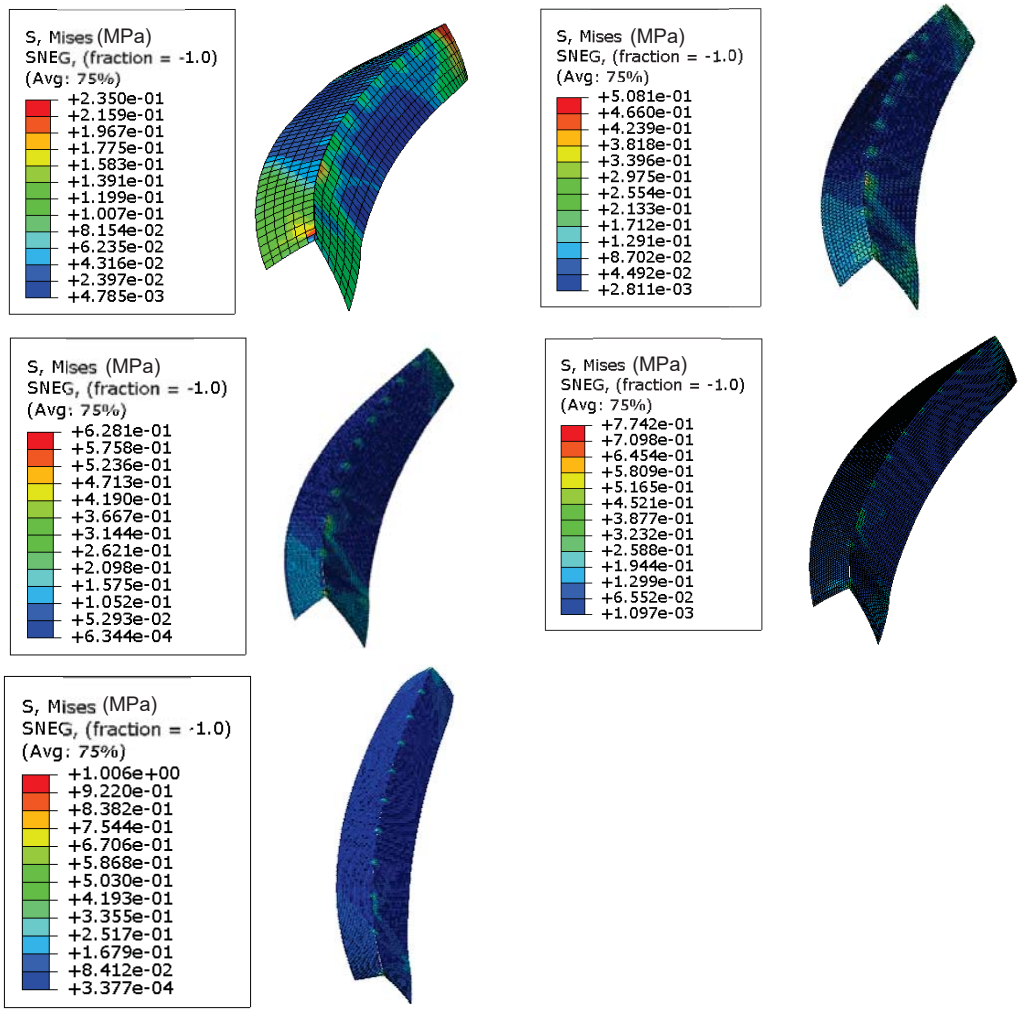

Fig. 6.4: Number of discretization along the crease (a) 50, (b) 100, (c) 150, (d) 200 and (e) 500

After the mesh sensitivity analysis, the next important quantification for the curved crease folding simulation is to identify the number of connector elements along the crease. This identification is important to find the most suitable number of connector elements for the selected curved crease curvature. This analysis is done for the same curved crease where discretized points are selected along the crease to construct the connectors as shown in Fig. 6.6 and 6.7.

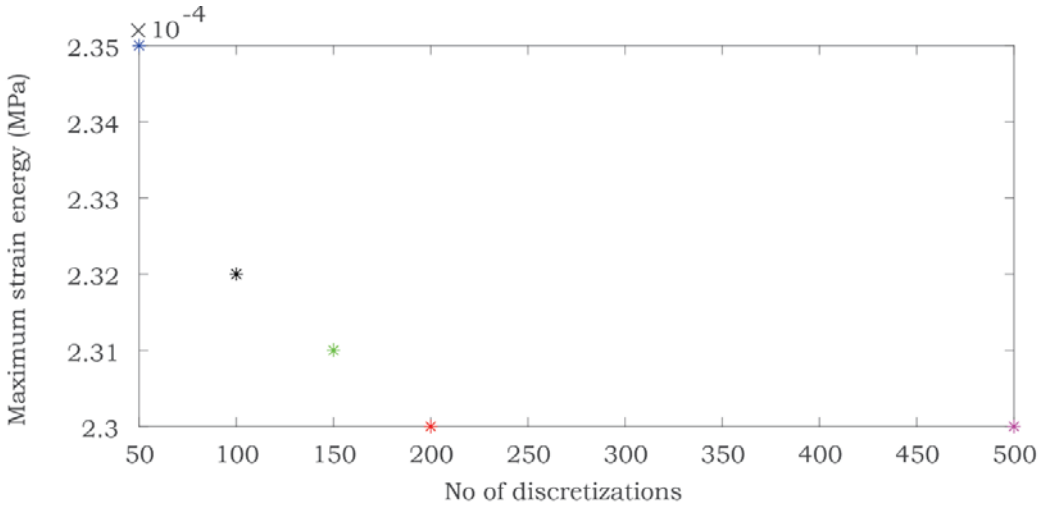

Fig. 6.5: Mesh sensitivity analysis for a curved crease

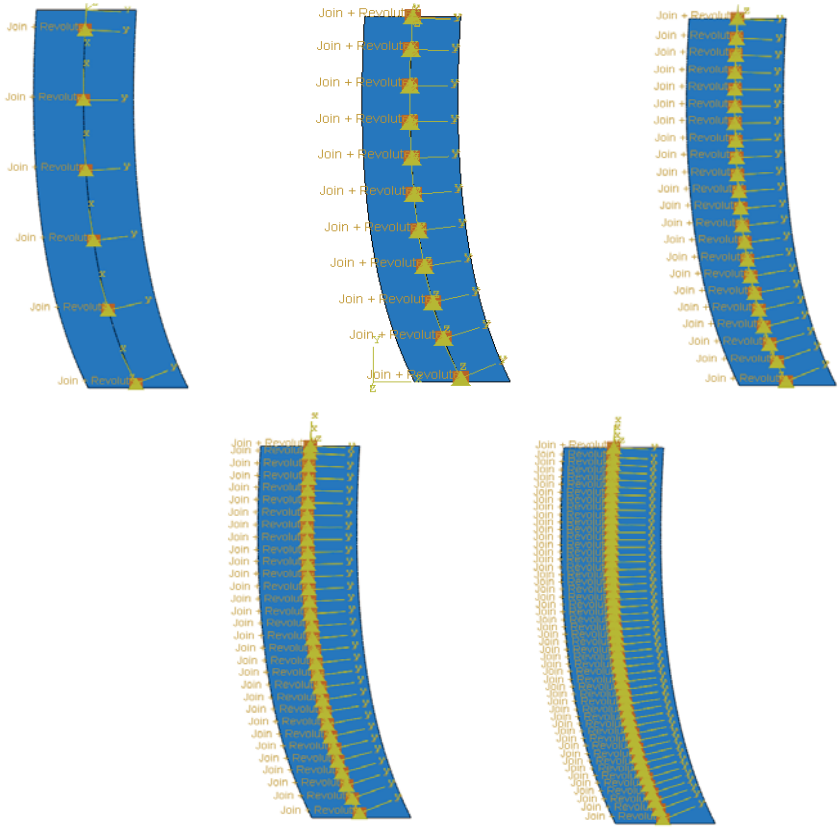

Fig. 6.6: Different connector arrangements with gaps of (a) 28 (b) 14 (c) 7 (d) 5 (e) 3

By changing the gap between the connectors there is five connector element numbers are selected for analysis. The gap between connectors along the crease varies as 28, 14, 7, 5, and 3 in the selected crease discretization of 200. The crease stiffness for the connectors was found by multiplying the distance between two connectors from the value 4.92778×10^{-7} N/degrees. After analyzing the strain energy variation, the gap between points along the crease is selected as 7 for the numerical model.

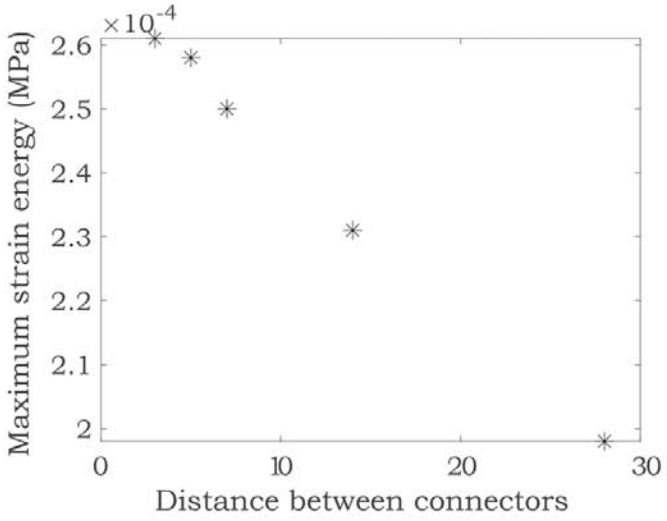

Fig. 6.7: Strain energy maximum value vs no of connector elements

6.3 Numerical Modelling of Wrapping Structure

The geometry constructed for the spiral folding pattern is used to generate the numerical model to analyze the wrapping structures. Two numerical models are constructed one for straight crease geometry and one for curved crease geometry as shown in Fig. 6.8. The numerical model is built according to the mesh sensitivity analysis and the connector distances prescribed in the previous subsections. To reduce the time taken for the analysis only one-sixth of the structure is selected for the analysis the central midpoint is pinned to restrain the movement and simulate the connection to the central hub.

In the numerical model, there are valley and ridge creases, and boundary conditions are distributed as in Fig. 6.9. The ridge creases are constrained to move in the Z direction and only allowed to move in the XY plane. The valley creases are given a displacement of 22 mm in the Z direction to fold the structure and are also allowed to move in the XY plane. The point where the panel connects to the central hub is simulated by assigning a pinned boundary condition at the vertices.

Along the two edges of the panels where it connects to other adjacent panels periodic boundary conditions are assigned simulating the panel behavior. The structure consists of 6 panels and to simulate a single-panel behavior the periodic boundary condition is assigned as follows,

-0.366 × translation in X direction at point 1 = translation in X direction at point 2

1.366 × translation in Y direction at point 1 = translation in Y direction at point 2

The translation in Z direction and rotations are not considered to reduce the constraint to the numerical model and to reduce the numerical model running time. Higher

constraints lead to higher processing time reducing time increments and drastically increasing the number of steps.

6.4 Numerical Model Results

The initial wrapping conditions of both straight and curved crease structures are observed in this study. The total wrapping simulation is 25 seconds and only the first 11 .5 seconds motion is recorded for the analysis. The wrapping simulation for the

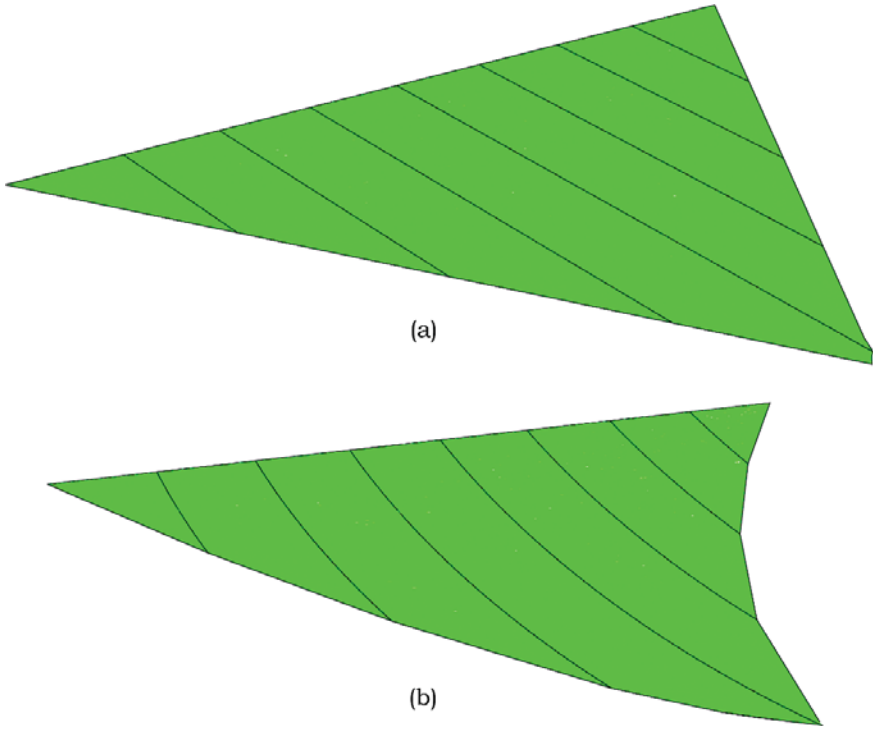

Fig. 6.8: Wrapping patterns (a) straight crease (b) curved crease

curved crease model is compared with the experimental results from Okuizumi et al [18]. The deployment rate is the ratio between the radius of the deployed surface to the actual radius of the membrane (0.325 m).The simulation results show a close variation in the initial region of the deployment but shows a little increment in the rate compared to the experimental results as in Fig. 6.10. This is because in experiments the membrane is deployed only to 0.9 times the actual radius due to gravity impacts but in simulation membrane is fully deployed.

In the initial stages, the straight crease model undergoes larger stresses along the crease regions as in Fig. 6.11. It is possible to observe 3- 26 percent stress reduction in the curved crease model during the observed initial wrapping motion. The straight crease structure has substantial stress concentrations along the creases and membrane panels during wrapping. Also, in the straight crease model during the initial folding stages, it is possible to observe that there are improper deformations in the stripes when they try to fold around the central hub. The membrane deformation only happens as linear crease folding due to straight crease geometry and when it tries to bend to

accommodate the wrapping higher stresses start to form. This damages the membrane structure and can cause improper wrapping around the central hub.

When this is compared with the curved crease spiral folding pattern it is possible to

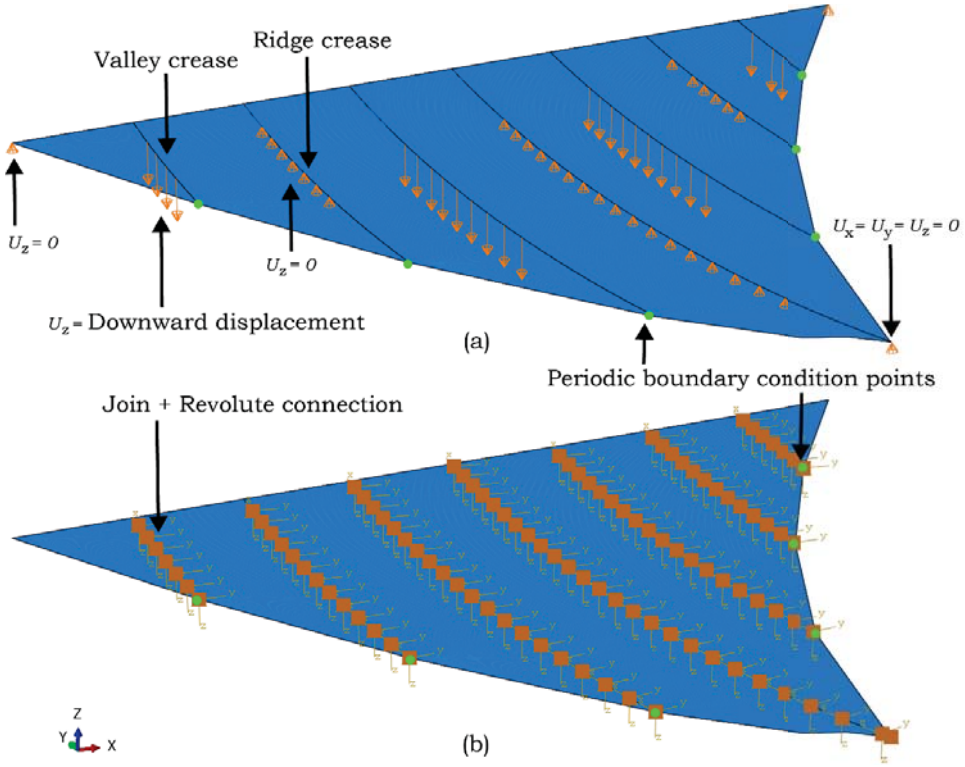

Fig. 6.9: Numerical model details (a) boundary conditions (b) connector arrangement

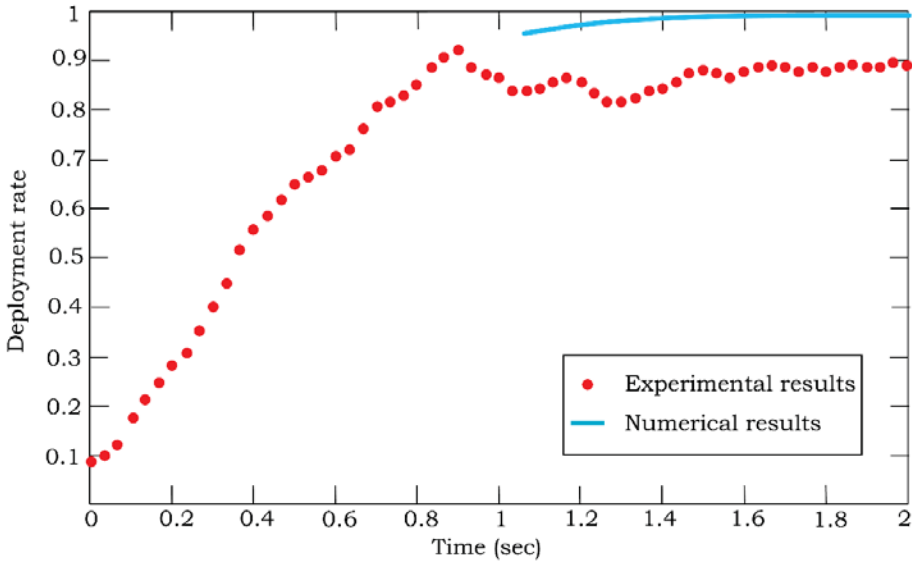

Fig. 6.10: Experimental vs numerical results

observe that with the folding the structure undergoes less stress value along the

membrane. With the applied displacement to fold the structure the creases start to fold, and the crease curvature starts to form. This helps to easily bend the crease geometry into a curved shape which helps to wrap around the central hub and the membrane inside the respective layers.

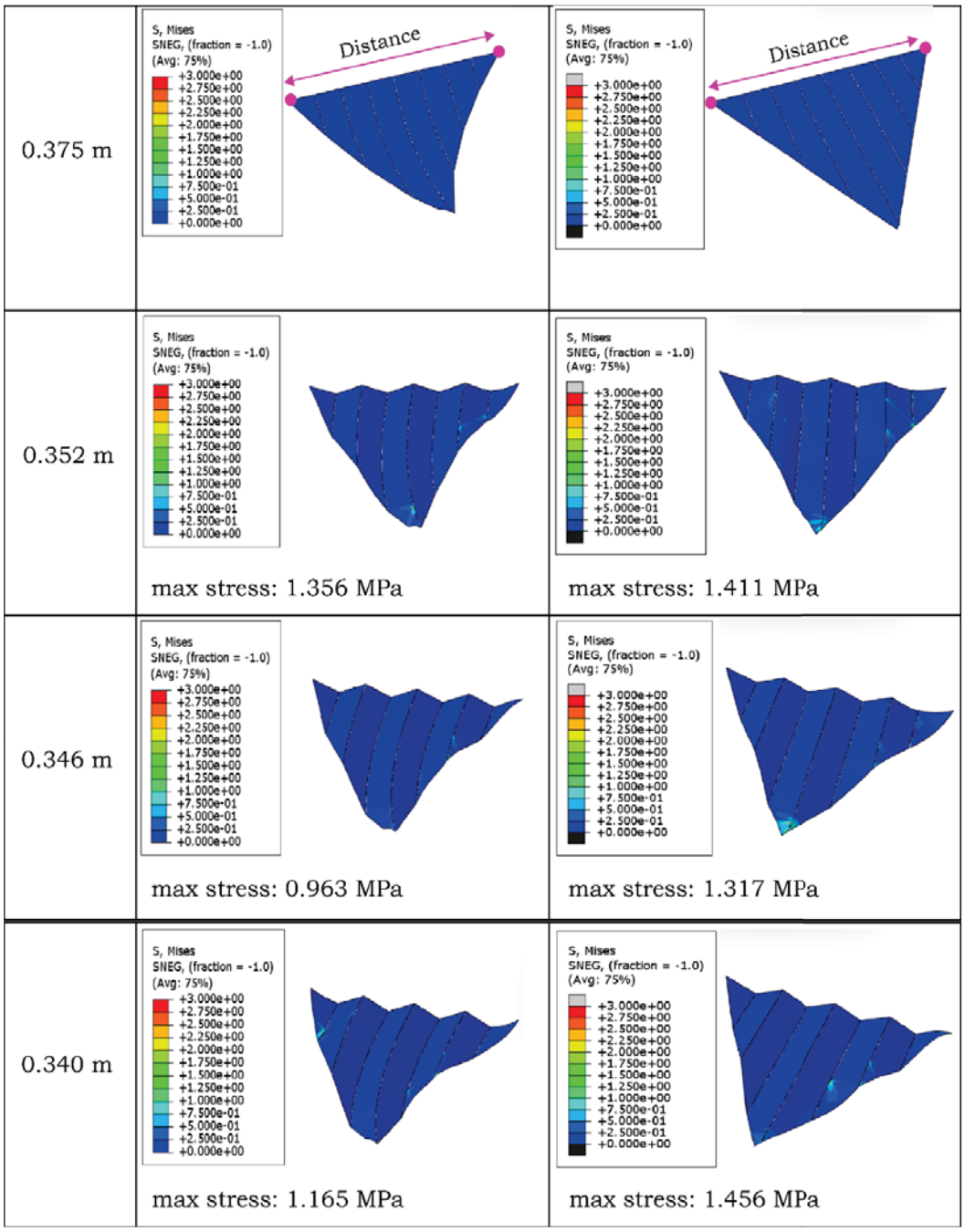

Fig. 6.11: Comparison of straight and curved crease numerical

CHAPTER 7

CONCLUSIONS AND FUTURE WORK

The focus of this research is to study deployable wrapping structures and to analyze the impact of changing creases from straight to curved. This changing crease geometry needs to be studied in the sense of stress distributions in the structure and folding geometry. Also, in membrane structures self-opening behavior is a key important feature. For an accurate demonstration, this also needs to be properly incorporated into numerical models. Therefore, a novel crease idealization technique is presented in the study to incorporate self-opening behavior into numerical models with multiple creases.

7.1 Conclusions from Self-opening Behavior Analysis

The self-opening behavior of a single crease is implemented into a multiple-creased numerical model and the idealization effectiveness is analyzed. This is analyzed in the sense of a Miura-Ori structure with 4 creases.

The numerical model results show a good overlap with experimental results. A slight deviation can be seen in the initial parts of the force vs displacement curves, but the overall fit can be considered acceptable. The force generated due to both folding and unfolding stages can be captured from this idealization by accurately showing the gradient change that occurred during the experiment.

This means the crease folding effect and the panel bending effect during the structure folding have also been captured with good accuracy. This idealization is required in the sense of modeling membrane structures that are integrated with creases. The self-opening behavior can be accurately implemented into numerical models with multiple creases which leads to accurate representation of its behavior in simulations. This idealization technique can be extended to accurately represent the self-opening behavior of structures with different materials not limited to membranes. The neutral angle and crease stiffness of the hinge are the only needed parameters to implement this to different structures with a self-opening crease.

7.2 Conclusions from Wrapping Pattern Analysis

In the wrapping pattern analysis, the curved crease model wrapping stages were compared with a straight crease numerical model. In the analysis of the results, it can be seen that in the initial stages, the straight crease pattern folds without much stress generated in the membrane. But when it tries to wrap around the central hub the membrane undergoes larger stress. When this is compared to the curved crease model the stresses are lesser than that of the straight crease model.

So, this concludes that the stresses generated in a curved crease model are lesser during the initial wrapping stage which is observed in this study. Also, when the geometry is

considered during the folding motion it is clear that the curved crease model provides a good overall wrapping motion. This concludes that in the sense of wrapping structures, it is beneficial to move into curved crease geometries which are constructed to accommodate the thickness increment during wrapping. This also benefits by reducing the stress generation in the membrane during the wrapping process and protects the membrane from damage due to stress concentrations. Also, this will lead to a more proper wrapping essentially giving a compacted wrapped structure.

7.3 Future Work

- In this study, the self-opening behavior of a single degree of freedom structure is analyzed. It is further recommended to analyze this behavior in a two-degree-of-freedom origami structure.
- Also, a structure with tessellations should be analyzed as most of the origami structures are constructed as tessellated structures. This further validates its implementation.
- The self-opening idealization of the crease is validated for a straight crease structure in this study. This can be implemented into a curved crease geometry and needs to be further analyzed for the accuracy of implementation for curved crease structures.
- The wrapping numerical model is only modeled with a crease stiffness value without incorporating a self-opening behavior. Further study should be conducted to analyze the self-opening behavior impact on modeling a wrapping simulation.
- In the wrapping simulation, one-sixth of the structure is only analyzed, and the total wrapping simulation is not analyzed. This needs to be done as a future study to accurately analyze the full curved crease wrapping behavior.

REFERENCES

[1] M. Chandra, S. Kumar, S. Chattopadhyaya, S. Chatterjee, and P. Kumar, "A review on developments of deployable membrane-based reflector antennas," *Advances in Space Research*, vol. 68, no. 9, pp. 3749–3764, Nov. 2021, doi: 10.1016/J.ASR.2021.06.051.

[2] G. Zhang, J. Wang, J. Guo, J. He, Y. Xu, and Y. Zhao, "A novel single-DoF deployable antenna mechanism based on heterogeneous modules: Configuration design and performance analysis," *Thin-Walled Structures*, vol. 203, p. 112232, Oct. 2024, doi: 10.1016/J.TWS.2024.112232.

[3] P. Zhao, C. Wu, and Y. Li, "Design and application of solar sailing: A review on key technologies," *Chinese Journal of Aeronautics*, vol. 36, no. 5, pp. 125–144, May 2023, doi: 10.1016/J.CJA.2022.11.002.

[4] B. Fu, E. Sperber, and F. Eke, "Solar Sail Technology-A State of the Art Review."

[5] T. W. Liu, J. B. Bai, N. Fantuzzi, and X. Zhang, "Thin-walled deployable composite structures: A review," *Progress in Aerospace Sciences*, vol. 146, p. 100985, Apr. 2024, doi: 10.1016/J.PAEROSCI.2024.100985.

[6] S. Wang, M. Schenk, S. Jiang, and A. Viquerat, "Blossoming analysis of composite deployable booms," *Thin-Walled Structures*, vol. 157, Dec. 2020, doi: 10.1016/j.tws.2020.107098.

[7] "XIN: Modeling and analysis of deployment dynamics... - Google Scholar." Accessed: Nov. 04, 2024. [Online]. Available: https://scholar.google.com/scholar_lookup?title=Modeling%20and%20analysis%20of%20deployment%20dynamics%20for%20UltraFlex%20solar%20array&publication_year=2020&author=P.%20Xin&author=Z.%20Liu&author=J.%20Rong&author=C.%20Liu&author=Z.%20Wu&author=B.%20Liu

[8] X. Lan *et al.*, "World's first spaceflight on-orbit demonstration of a flexible solar array system based on shape memory polymer composites," *Sci China Technol Sci*, vol. 63, no. 8, pp. 1436–1451, Aug. 2020, doi: 10.1007/s11431-020-1681-0.

[9] P. Seefeldt, J. T. Grundmann, M. Hillebrandt, and M. Zander, "Performance analysis and mission applications of a new solar sail concept based on crossed booms with tip-deployed membranes," *Advances in Space Research*, vol. 67, no. 9, pp. 2736–2745, May 2021, doi: 10.1016/j.asr.2020.10.001.

[10] C. Wang, H. Guo, R. Liu, and Z. Deng, "A programmable origami-inspired space deployable structure with curved surfaces," *Eng Struct*, vol. 256, p. 113934, Apr. 2022, doi: 10.1016/J.ENGSTRUCT.2022.113934.

[11] G. Kiper and E. Söylemez, “Deployable space structures,” in *RAST 2009 - Proceedings of 4th International Conference on Recent Advances Space Technologies*, 2009, pp. 131–138. doi: 10.1109/RAST.2009.5158183.

[12] J. He, Y. Zhang, Z. Shangguan, and L. Yang, “A Review of Bionic Design in Satellite Solar Wing Structures,” *J Phys Conf Ser*, vol. 1549, no. 4, Jun. 2020, doi: 10.1088/1742-6596/1549/4/042099.

[13] S. Yu, J. Liu, P. Zhao, and Y. Tang, “A flat-foldable equiangular spiral folding pattern inspired by sunflowers for deployable structures,” *Chinese Journal of Aeronautics*, vol. 37, no. 6, pp. 425–438, Jun. 2024, doi: 10.1016/j.cja.2023.10.004.

[14] P. M. Liyanage, N. Gangasudan, and H. M. Y. C. Mallikarachchi, “Modified spiral folding pattern for deployable membranes,” *Aerosp Sci Technol*, vol. 117, p. 106926, Oct. 2021, doi: 10.1016/J.AST.2021.106926.

[15] H. Sakamoto *et al.*, “Folding patterns of planar gossamer space structures consisting of membranes and booms,” *Acta Astronaut*, vol. 94, no. 1, pp. 34–41, 2014, doi: https://doi.org/10.1016/j.actaastro.2013.07.036.

[16] G. Greschik and M. M. Mikulas, “Design Study of a Square Solar Sail Architecture,” *J Spacecr Rockets*, vol. 39, no. 5, pp. 653–661, 2002, doi: 10.2514/2.3886.

[17] M. Arya, N. Lee, and S. Pellegrino, “Crease-free biaxial packaging of thick membranes with slipping folds,” *Int J Solids Struct*, vol. 108, pp. 24–39, 2017, doi: https://doi.org/10.1016/j.ijsolstr.2016.08.013.

[18] N. Okuizumi and T. Yamamoto, “Centrifugal Deployment of Membrane with Spiral Folding: Experiment and Simulation,” *Journal of Space Engineering*, vol. 2, no. 1, pp. 41–50, 2009, doi: 10.1299/spacee.2.41.

[19] S. Guest and S. Pellegrino, “Inextensional wrapping of flat membranes,” *Proceedings of International Seminar Structure Morphology*, Aug. 1992.

[20] Y. Tsuda *et al.*, “Achievement of IKAROS — Japanese deep space solar sail demonstration mission,” *Acta Astronaut*, vol. 82, no. 2, pp. 183–188, Feb. 2013, doi: 10.1016/J.ACTAASTRO.2012.03.032.

[21] M. C. Natori, N. Kishimoto, H. Watanabe, and K. Higuchi, “Morphological Concepts on Efficient Space Structures with Deployable and/or Adaptive Functions,” 2008.

[22] M. C. Natori, N. Katsumata, and H. Yamakawa, “Membrane Modular Space Structures and Deployment Characteristics of Their Inflatable Tube Elements,” in *51st AIAA/ASME/ASCE/AHS/ASC Structures, Structural Dynamics, and Materials Conference*. doi: 10.2514/6.2010-2909.

[23] H. Kobayashi, B. Kresling, and J. F. V Vincent, “The geometry of unfolding tree leaves,” *Proc R Soc Lond B Biol Sci*, vol. 265, no. 1391, pp. 147–154, 1998, doi: 10.1098/rspb.1998.0276.

[24] N. Lee and S. Pellegrino, “Multi-Layered Membrane Structures with Curved Creases for Smooth Packaging and Deployment.”

[25] N. Lee and S. Close, “Curved pleat folding for smooth wrapping,” *Proceedings of the Royal Society A: Mathematical, Physical and Engineering Sciences*, vol. 469, no. 2155, p. 20130152, 2013, doi: 10.1098/rspa.2013.0152.

[26] S. R. Woodruff and E. T. Filipov, “Bending and twisting with a pinch: Shape morphing of creased sheets,” *Extreme Mech Lett*, vol. 52, p. 101656, 2022, doi: https://doi.org/10.1016/j.eml.2022.101656.

[27] V. Parque and T. Miyashita, “On spiral folding of planar membranes with finite thickness and curved creases,” 2022. [Online]. Available: http://asmedigitalcollection.asme.org/IDETC-CIE/proceedings-pdf/IDETC-CIE2022/86236/V03BT03A016/6943216/v03bt03a016-detc2022-90145.pdf

[28] A. Ghassaei, E. D. Demaine, and N. A. Gershenfeld, “Fast , Interactive Origami Simulation using GPU Computation,” 2018. [Online]. Available: https://api.semanticscholar.org/CorpusID:52839481

[29] Q. Lin *et al.*, “Wrapping Deployment Simulation Analysis of Leaf-Inspired Membrane Structures,” *Aerospace*, vol. 8, no. 8, 2021, doi: 10.3390/aerospace8080218.

[30] S. Mierunalan, S. P. Dassanayake, H. M. Y. C. Mallikarachchi, and S. H. Upadhyay, “Simulation of ultra-thin membranes with creases,” *International Journal of Mechanics and Materials in Design*, vol. 19, no. 1, pp. 73–94, 2023, doi: 10.1007/s10999-022-09617-6.

[31] N. Sutharsanan and H. M. Y. C. Mallikarachchi, “Characterising self-opening behaviour of single creased kapton polyimide films,” 2021.